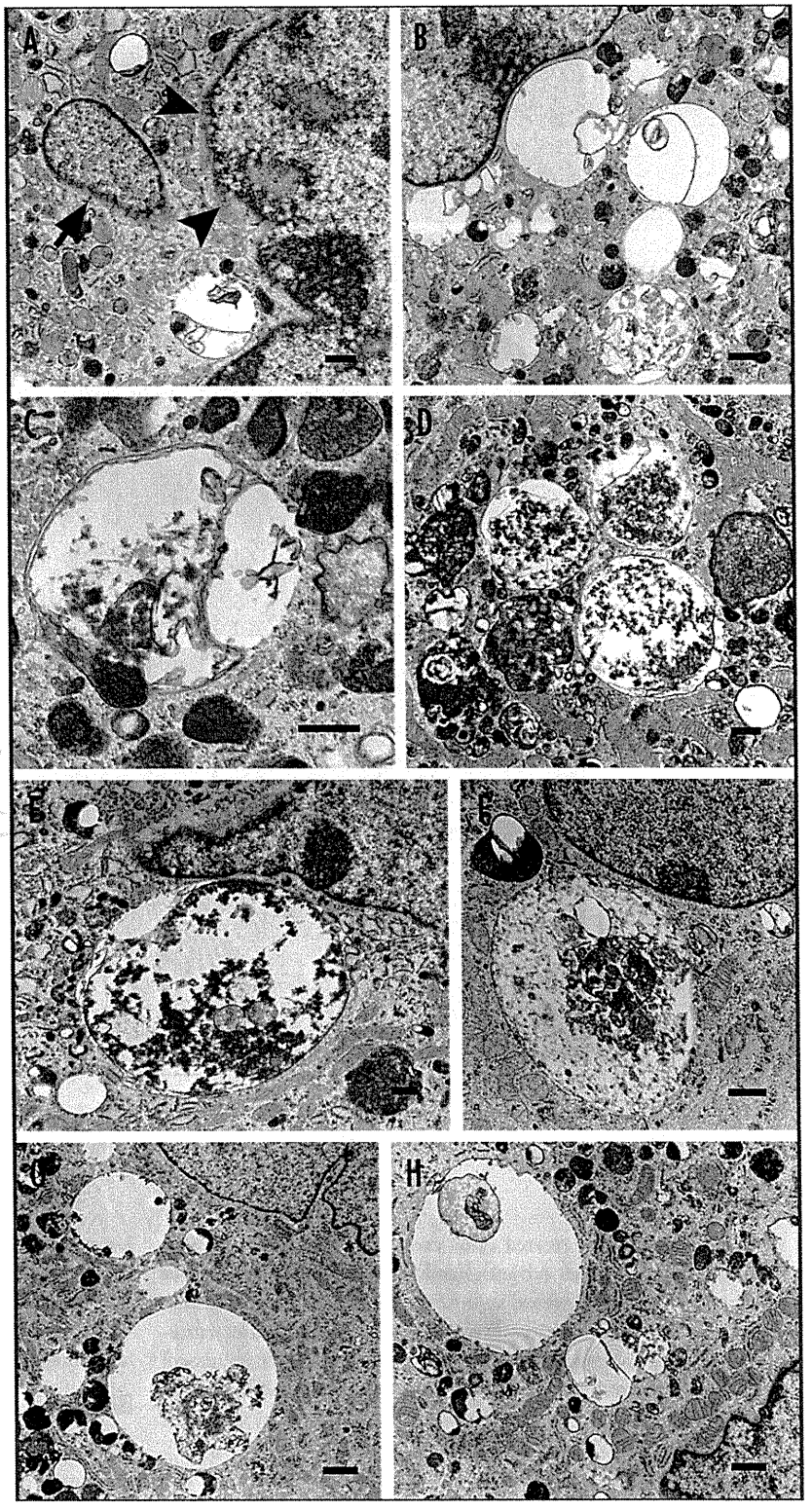

Figure 5. Characterization of nuclear components contained in the GFP-positive autophagosomes on immunocytochemistry. (A–C) GFP-positive autophagosomes with variable sized are seen close to the nuclei, and most of which are partially colocalized with DAPI signals outside of nucleus. Extranuclear DAPI signals in the GFP-positive autophagosomes are positive for histone H1 (A), but not for nuclear envelope proteins such as lamin A and B (B and C). (D) Extranuclear DAPI signals with GFP staining are positive for γH2AX (arrowhead). (E) Nuclear fragments with scattered γH2AX staining are negative for LC3.

pattern between GFP and LC3 despite their essential identity is probably due to the accumulation of GFP that is resistant to lysosomal hydrolase. Further immunostaining of other autophagy-related proteins (i.e., Atg5, 16L, 9 and Rab7) and LAMP2 confirmed that the GFP-positive signals are ultimately autophagosomes and autolysosomes. Our findings indicate that the autophagosomes appear to degrade the extruded nuclear components since most of them contained extranuclear DAPI and major histone protein H1 within. Irregularly blurred or faint DAPI or H1 signals inside the autophagosomes/autolysosomes substantiate that nuclear components are being degraded by autophagic process. The target of autophagy is probably the damaged portions of nuclei as demonstrated by γH2AX immunostaining.

Electron microscopic observations of $Lmna^{H222P/H222P}$ cells demonstrated that autophagosomes were clustered and lysosomes fused to form giant autophagosomes, which were sometimes bigger than nuclei. Giant autophagosomes are quite unusual and are rarely seen in starvation-induced autophagy, where the size is about 1 μm.[35] Similar large-sized (5 to 10 μm) autophagosomes has been reported to encircle bacteria in HeLa cells under group A streptococcus infection although the mechanism to form such giant autophagosomes was not clarified.[41] From our findings it can be suggested that the formation of giant autophagosomes may be required for the degradation of large molecules, such as a part of nucleus.

We propose that $Lmna^{H222P/H222P}$ nuclei, having incomplete lamina structure and frequently subjected to mechanical stress, subsequently become damaged and would apparently require (giant) autophagosome for degradation by lysosomal enzymes. Thus, it seems that this nuclear autophagy is consistent with macroautophagy in terms of its morphology and machinery used. On the other hand, piecemeal microautophagy of nucleus (PMN) has been recently

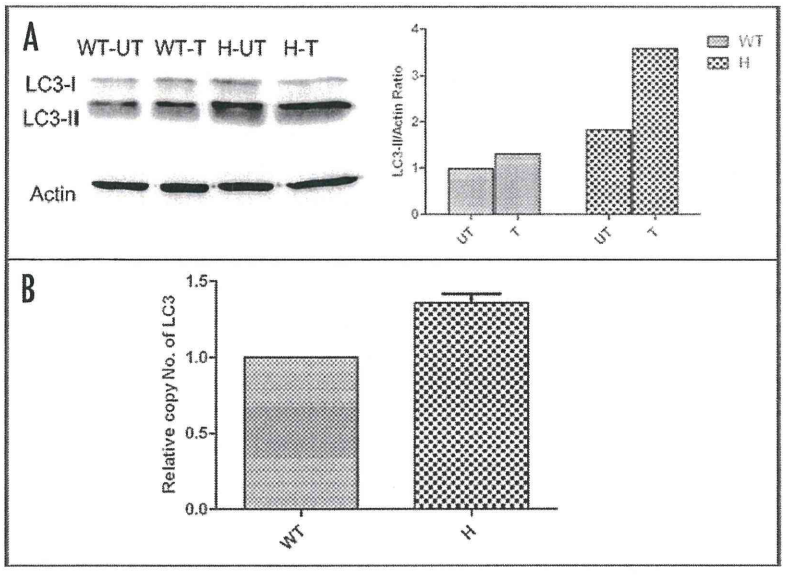

Figure 6. Immunoblotting analysis of LC3 and quantitative real-time PCR of *Maplc3b*. (A) The amount of LC3-II is highly increased in *Lmna*$^{H222P/H222P}$ cells, and which gets more increased with the treatment of lysosomal protease inhibitors (pepstatin A and E64d), suggesting that autophagy is markedly activated in the diseased cells. (B) By quantitative real-time PCR of *Maplc3b*, the transcriptional level of LC3 is represented to be significantly increased in *Lmna*$^{H222P/H222P}$ MEF compared with wild-type ($p = 0.0141$). WT-UT, untreated wild-type; WT-T, treated wild-type; H-UT, untreated *Lmna*$^{H222P/H222P}$; H-T, treated *Lmna*$^{H222P/H222P}$ cells.

reported in *S. cerevisiae*, which is induced by nutritional depletion or rapamycin stimulation. During PMN velcro-like patches are formed by the interaction between vacuolar membrane and outer nuclear membrane at nonessential portions of nuclei.[42] PMN is morphologically categorized as microautophagy because nuclear components are directly engulfed by vacuoles without formation of vesicular intermediates, i.e., autophagosome.[43,44] This concept was further supported by a recent investigation that elucidated the core machinery on PMN.[44] Because detailed underlying molecular mechanism is still unclear, we could not completely exclude the possible involvement of microautophagy for degradation of nuclear blebs observed in *Lmna*$^{H222P/H222P}$ cells.

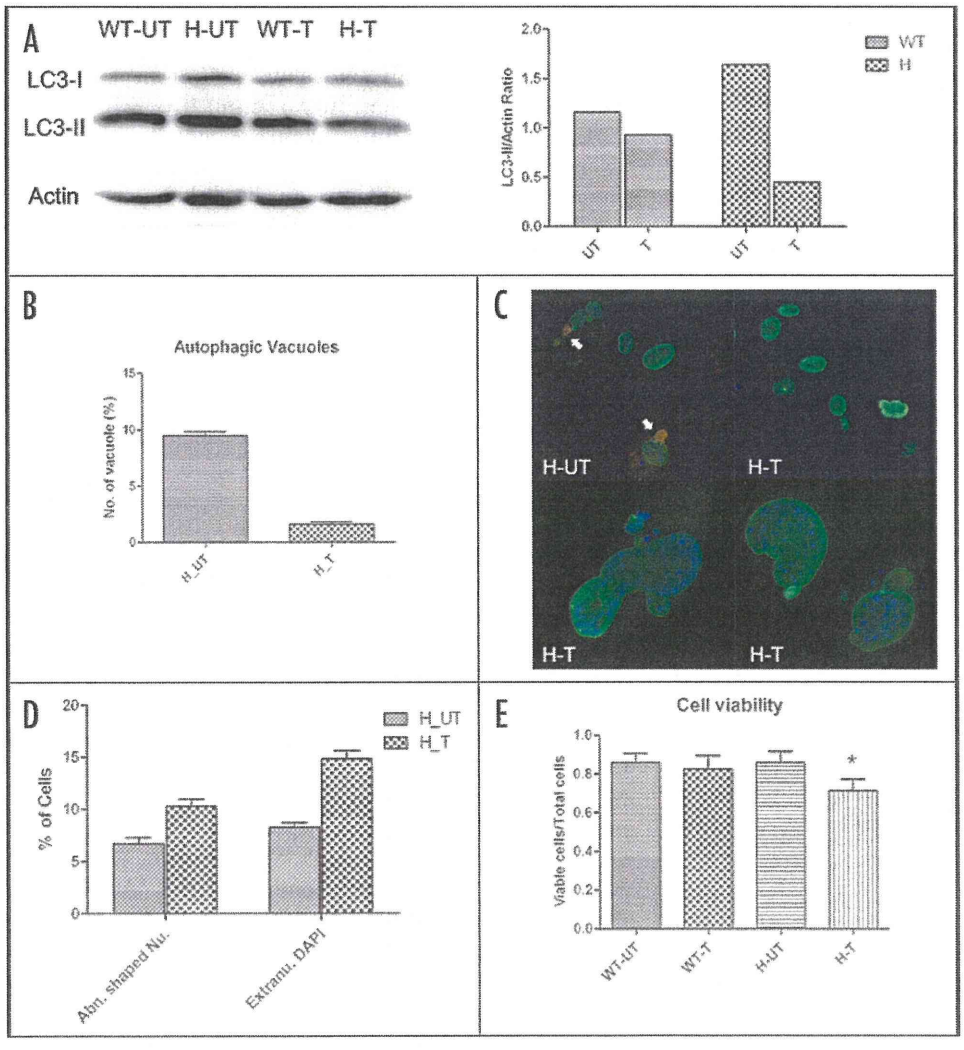

Figure 7. Changes in nuclear abnormalities and cell survival rate after autophagy inhibition. (A) Immunoblotting analysis of LC3 shows that LC3-II is decreased after autophagy inhibition in wild-type and *Lmna*$^{H222P/H222P}$ cells. (B) In treated *Lmna*$^{H222P/H222P}$ cells, autophagic vacuoles are significantly decreased compared with untreated cells ($p < 0.0001$). (C) On immunocytochemistry of LC3 (red), lamin C (green) and DAPI (blue), the treated *Lmna*$^{H222P/H222P}$ cells rarely show LC3 staining whereas untreated cells frequently display perinuclear autophagosomes (arrows, upper). With autophagy inhibition, cells present severe deformation of nuclei and multiple extranuclear DAPI (lower). (D) The number of cells with markedly irregular shaped nuclei and extranuclear DAPI is much increased by autophagy inhibition ($p = 0.0008$) (E) Cell viability assay represents the decreased cell survival rate in *Lmna*$^{H222P/H222P}$ cells by autophagy inhibition compared with wild-type cells (*$p = 0.0029$). WT, wild-type; H, *Lmna*$^{H222P/H222P}$; UT, untreated; T, treated.

The activation of autophagy in *Lmna*$^{H222P/H222P}$ cells is supported by the finding of increased amount of LC3-II on immunoblotting analysis, and the transcriptional upregulation of LC3 expression. LC3 has been previously reported to be increased in progeroid mice lacking zinc metalloproteinase STE24 or ZMPSTE24 (*Zmpste24*$^{-/-}$),[45] an enzyme required for the maturation of lamin A. ZMPSTE24 deficiency causes accumulation of the premature form of lamin A (prelamin A) in nuclear envelope and leads to profound nuclear architecture abnormalities.[46] Increased LC3 was thought to be secondary to enhanced basal autophagy in skeletal and cardiac muscles due to a metabolic derangement in progeroid mice. Considering similar molecular defects of nuclear lamina in two mouse models of *Zmpste24*$^{-/-}$ and *Lmna*$^{H222P/H222P}$, we cannot totally exclude the possibility of increased basal autophagy in *Lmna*$^{H222P/H222P}$ mice although they did not show comparable alterations in glucose and lipid metabolism.[47] In this study, the finding that GFP-LC3-positive vacuoles were consistently related to the cytoplasmic nuclear components could indicate that activated autophagy in *Lmna*$^{H222P/H222P}$ cells may at least in part be induced by the nuclear damage.

Reduced cell viability in *Lmna*$^{H222P/H222P}$ cells after autophagy inhibition probably resulted from increased frequency of nuclear abnormalities as shown in Figure 7. This result ultimately indicates that autophagy is working for the maintenance of cellular homeostasis by cleaning up nuclear wastes in *Lmna*$^{H222P/H222P}$ cells. With autophagic degradation of nuclear components, however, a partial loss of genetic information may be inevitable, leading to a varying degree of molecular defects on cells. Cells with bulk loss of genetic materials can be thought to eventually undergo apoptosis, but clarification of this issue is beyond the scope of this paper.

In conclusion, we have demonstrated the presence of perinuclear autophagosomes/autolysosomes in *Lmna*$^{H222P/H222P}$ cells. Notably, in the area of nuclear membrane interfacing with autophagosomes/autolysosomes, we could see accumulation of nuclear envelope proteins. This may suggest that autophagy could contribute to the rapid repair of the nuclear membrane, as there is a need to rescue the cells from overdegradation or to minimize the loss of nuclear components after nuclear membrane injury. This would be worth exploring in future experiments.

It is also notable that similar autophagosomes/autolysosomes containing nuclear components were found even in wild-type cells although to a much lower frequency. This implies that autophagic degradation of nuclear components is not confined to nuclear envelopathy, and can occur under other conditions that cause nuclear damage. Like other organelle-specific autophagy reported to date, the autophagy in *Lmna*$^{H222P/H222P}$ MEF can be proposed to be called as 'nucleophagy.' Nevertheless, the precise role of "nucleophagy" in laminopathies, and possibly in physiologic conditions, remains perplexing and a potential interest that needs to be elucidated.

Materials and Methods

Mouse models for nuclear envelopathy and generation of *Lmna*$^{H222P/H222P}$*/GFP-LC3* transgenic mouse. We used H222P homozygous knock-in (*Lmna*$^{H222P/H222P}$),[47] *Lmna* knockout (*Lmna*$^{-/-}$),[48] and emerin knockout (*Emd*$^{-/-}$) mice[25] as mouse models for nuclear envelopathy in this study. The mutation of p.H222P in *LMNA* is one of the mutations causing muscular dystrophy in human, and the homozygous mouse model carrying the mutation, *Lmna*$^{H222P/H222P}$ reproduced the phenotype of human muscular dystrophy due to *LMNA* mutations.[47] *Lmna*$^{-/-}$ mice have shown postnatal lethality in addition to muscular dystrophy and cardiomyopathy although they were normal at birth.[48] *Emd*$^{-/-}$ mice demonstrated altered motor coordination and delayed atrioventricular conduction time in electrocardiogram, but overall they showed normal growth rate and were without obvious muscle weakness.[25]

Lmna$^{H222P/H222P}$ mice were crossed with GFP-LC3 transgenic mice[35] (kindly provided by Dr. Mizushima in Tokyo Medical and Dental University) to generate *Lmna*$^{H222P/H222P}$*/GFP-LC3* transgenic mice.

Electron microscopic observation. Soleus muscles and skin of abdomen obtained from *Lmna*$^{H222P/H222P}$ mice and wild-type littermates were obtained for electron microscopic observation. Tissues were fixed with 2% glutaraldehyde in 0.1 M cacodylate buffer. After shaking with a mixture of 4% osmium tetroxide, 1.5% lanthanum nitrate and 0.2 M s-collidine for 2 hours, samples were embedded in epoxy resin.

Lmna$^{H222P/H222P}$ MEF were cultured and grown on Lab-Tek^{TM} chambered coverglass (Nunc, Tokyo, Japan). They were fixed with 1.2% glutaraldehyde in 0.1 M phosphate buffer (pH 7.4) at 4°C for one hour. After osmification of cells with 1% OsO4 in 0.1 M phosphate buffer at 4°C, they were embedded in epoxy resin.

Ultrathin sections (50 nm thickness) were stained with uranyl acetate and lead citrate, and then examined under H-600 transmission electron microscope (Hitachi, Japan) at 75 kV.

Cell culture and immunocytochemistry. Mouse embryonic fibroblasts (MEF) were obtained from *Lmna*$^{H222P/H222P}$, *Lmna*$^{-/-}$, *Lmna*$^{H222P/H222P}$*/GFP-LC3* transgenic mice and wild-type littermates. They were harvested in 100-mm collagen I-coated dishes with Dulbecco's modified Eagle medium (DMEM, Wako, Osaka, Japan) containing 10% fetal bovine serum (FBS) and 1% of antibiotics, and incubated at 37°C in humidified chamber with 5% CO_2.

Cultured cells were plated on collagen I-coated glass coverslips and fixed with 4% paraformaldehyde in PBS for 15 min at 4°C, permeabilized on ice with 0.25% Triton X-100/PBS for 20 min, blocked with 2% casein/PBS for 15 min at 37°C, and then immunostained with primary antibodies diluted in 2% casein/PBS for 2 hrs at 37°C. Primary antibodies used in this study are as follows: anti-lamin A (Abcam, Tokyo, Japan), lamin C,[16] lamin B (Santa Cruz Biotechnology Inc., CA), emerin (Novocastra Laboratories, Newcastle upon Tyne, UK), lamin-associated protein 2α (LAP2α), nesprin 1α (Abcam, Tokyo, Japan), LC3 (provided by Dr. Ueno, Juntendo university), Atg5 (Sigma-Aldrich, Tokyo, Japan), Atg9 (Biosensis, Thebarton, South Australia), Atg16L, Rab7 (Sigma-Aldrich), LAMP2 (Developmental Studies Hybridoma Bank), histone H1 (Santa Cruz Biotechnology Inc.,), H2AX (Abcam). Cells were then incubated with fluorescently labeled secondary antibodies (Alexa488 or Alexa568) at room temperature

for 45 min. Coverslips were mounted together with 4',6-diamidino-2-phenylindole (DAPI, Invitrogen, CA) for nuclear localization, and then visualized under epifluorescence using Axiophoto II (Carl Zeiss).

To detect lysosomal localization, cells were incubated with PBS containing 100 nM of Lyso-Tracker® (Invitrogen) at 37°C for 1 hour. After rinsing with PBS, cells were fixed with 4% paraformaldehyde at 37°C for 20 min.

Immunoblotting analysis of LC3. *Lmna*$^{H222P/H222P}$ and wild-type MEF were grown on 100 mm-collagen I coated dishes. At 80% confluent state, cells were treated with lysosomal protease inhibitors consisting of pepstatin A (20 μg/mL, Peptide Institute, Osaka, Japan) and E64d (20 μg/mL, Peptide Institute), or with dimethylsulfoxide (DMSO) as a negative control for 4 hours. Whole cell lysates was extracted with lysis buffer (1% NP-40 cell lysis buffer supplemented with protease inhibitor). Immunoblotting analysis of LC3 was performed according to the standard method. Twenty micrograms of protein of each sample were loaded on 12.5% sodium dodecyl sulfate-polyacrylamide gel. After electrophoresis, the gel was transferred to polyvinylidene (PVDF) membrane and immunostained with anti-LC3 antibody. Data was analyzed by using LAS-1000 chemiluminescence imaging system (Fujifilm, Tokyo, Japan).

Quantitative real-time PCR. Total RNA was extracted from *Lmna*$^{H222P/H222P}$ and wild-type MEF with TRIzol (Invitrogen) following manufacturer's protocol. Single-stranded cDNA was synthesized from RNA using SuperScript™ III reverse transcriptase. Gene expression of LC3B was quantified by quantitative real-time PCR in Rotor-Gene™ 6000 system (Corbett Life Science, NSW, Australia), using the following primers: LC3b-F; CCG AGA AGA CCT TCA AGC AG and LC3b-R; CCA TTC ACC AGG AGG AAG AA. All the results were normalized with respect to G3PDH expression.

Autophagy inhibition. MEF from *Lmna*$^{H222P/H222P}$ mice and wild-type littermates were treated with 10 mM 3-MA (Sigma-Aldrich) and 200 nM wortmannin (Sigma-Aldrich), which are also known as phosphatidylinositol-3 kinase inhibitors and autophagy inhibitors, or negative control at 80% confluent state for 2 hours as previously described.[49] After the treatment, the amount of LC3 was measured by immunoblotting analysis. Immunocytochemistry of LC3 and a nuclear envelope protein (lamin C) was also performed to check the changes in nuclear abnormalities with autophagy inhibition. For the calculation of cell survival rate, the cells were stained by acetoxymethyl ester of calcein (Calcein-AM, Dojindo, MD) and propidium iodine (PI, Dojindo) for 15 min at 37°C according to the manufacturer's instruction. This staining method can differentiate green-colored viable and red-colored dead cells, respectively. Cell viability was determined as the ratio of the number of viable cells per total number of cells in four groups of untreated wild-type, treated wild-type, untreated *Lmna*$^{H222P/H222P}$ and treated *Lmna*$^{H222P/H222P}$ cells.

Statistical analyses. To get quantitative data, three to four replicates of measurement were done for each condition. All the data were presented as mean and standard deviation. Comparisons among groups were done by using student-t test and analysis of variance (ANOVA) as appropriate. Statistical significance was considered when p value was less than 0.05.

Acknowledgements

We thank Drs. Colin L. Stewart (National Cancer Institute, MD, USA) and Dr. Noboru Mizushima (Tokyo Medical and Dental University, Tokyo) for providing mice of Lmna$^{-/-}$ and GFP-LC3, respectively, and Dr. May Christine V. Malicdan (National Institute of Neuroscience, NCNP) for reviewing the manuscript. This study was supported by the "Research on Psychiatric and Neurological Diseases and Mental Health" of "Health Labour Sciences Research Grant" and the "Research Grant (20B-12, 20B-13) for Nervous and Mental Disorders" from the Ministry of Health, Labor and Welfare; Human Frontier Science Program; Grant-in-Aid for Scientific Research from Japan Society for the Promotion of Science; Research on Publicly Essential Drugs and Medical Devices from the Japanese Health Sciences Foundation; and Program for Promotion of Fundamental Studies in Health Sciences of the National Institute of Biomedical Innovation (NIBIO).

Note

Supplementary materials can be found at:
www.landesbioscience.com/supplement/ParkAUTO5-6-Sup.pdf

References

1. Bonne G, Di Barletta MR, Varnous S, Becane HM, Hammouda EH, Merlini L, et al. Mutations in the gene encoding lamin A/C cause autosomal dominant Emery-Dreifuss muscular dystrophy. Nat Genet 1999; 21:285-8.
2. Raffaele Di Barletta M, Ricci E, Galluzzi G, Tonali P, Mora M, Morandi L, et al. Different mutations in the LMNA gene cause autosomal dominant and autosomal recessive Emery-Dreifuss muscular dystrophy. Am J Hum Genet 2000; 66:1407-12.
3. Muchir A, Bonne G, van der Kooi AJ, van Meegen M, Baas F, Bolhuis PA, et al. Identification of mutations in the gene encoding lamins A/C in autosomal dominant limb girdle muscular dystrophy with atrioventricular conduction disturbances (LGMD1B). Hum Mol Genet 2000; 9:1453-9.
4. Fatkin D, MacRae C, Sasaki T, Wolff MR, Porcu M, Frenneaux M, et al. Missense mutations in the rod domain of the lamin A/C gene as causes of dilated cardiomyopathy and conduction-system disease. N Engl J Med 1999; 341:1715-24.
5. Becane HM, Bonne G, Varnous S, Muchir A, Ortega V, Hammouda EH, et al. High incidence of sudden death with conduction system and myocardial disease due to lamins A and C gene mutation. Pacing Clin Electrophysiol 2000; 23:1661-6.
6. Cao H, Hegele RA. Nuclear lamin A/C R482Q mutation in canadian kindreds with Dunnigan-type familial partial lipodystrophy. Hum Mol Genet 2000; 9:109-12.
7. De Sandre-Giovannoli A, Chaouch M, Kozlov S, Vallat JM, Tazir M, Kassouri N, et al. Homozygous defects in LMNA, encoding lamin A/C nuclear-envelope proteins, cause autosomal recessive axonal neuropathy in human (Charcot-Marie-Tooth disorder type 2) and mouse. Am J Hum Genet 2002; 70:726-36.
8. De Sandre-Giovannoli A, Bernard R, Cau P, Navarro C, Amiel J, Boccaccio I, et al. Lamin a truncation in Hutchinson-Gilford progeria. Science 2003; 300:2055.
9. Eriksson M, Brown WT, Gordon LB, Glynn MW, Singer J, Scott L, et al. Recurrent de novo point mutations in lamin A cause Hutchinson-Gilford progeria syndrome. Nature 2003; 423:293-8.
10. Bione S, Maestrini E, Rivella S, Mancini M, Regis S, Romeo G, Toniolo D. Identification of a novel X-linked gene responsible for Emery-Dreifuss muscular dystrophy. Nat Genet 1994; 8:323-7.
11. Ura S, Hayashi YK, Goto K, Astejada MN, Murakami T, Nagato M, et al. Limb-girdle muscular dystrophy due to emerin gene mutations. Arch Neurol 2007; 64:1038-41.
12. Karst ML, Herron KJ, Olson TM. X-linked nonsyndromic sinus node dysfunction and atrial fibrillation caused by emerin mutation. J Cardiovasc Electrophysiol 2008; 19:510-5.
13. Ben Yaou R, Toutain A, Arimura T, Demay L, Massart C, Peccate C, et al. Multitissular involvement in a family with LMNA and EMD mutations: Role of digenic mechanism? Neurology 2007; 68:1883-94.
14. Broers JL, Peeters EA, Kuijpers HJ, Endert J, Bouten CV, Oomens CW, et al. Decreased mechanical stiffness in LMNA$^{-/-}$ cells is caused by defective nucleo-cytoskeletal integrity: implications for the development of laminopathies. Hum Mol Genet 2004; 13:2567-80.

15. Lammerding J, Schulze PC, Takahashi T, Kozlov S, Sullivan T, Kamm RD, et al. Lamin A/C deficiency causes defective nuclear mechanics and mechanotransduction. J Clin Invest 2004; 113:370-8.
16. Sakaki M, Koike H, Takahashi N, Sasagawa N, Tomioka S, Arahata K, Ishiura S. Interaction between emerin and nuclear lamins. J Biochem 2001; 129:321-7.
17. Mislow JM, Holaska JM, Kim MS, Lee KK, Segura-Totten M, Wilson KL, McNally EM. Nesprin-1alpha self-associates and binds directly to emerin and lamin A in vitro. FEBS Lett 2002; 525:135-40.
18. Bengtsson L, Wilson KL. Multiple and surprising new functions for emerin, a nuclear membrane protein. Curr Opin Cell Biol 2004; 16:73-9.
19. Zhang Q, Ragnauth CD, Skepper JN, Worth NF, Warren DT, Roberts RG, et al. Nesprin-2 is a multi-isomeric protein that binds lamin and emerin at the nuclear envelope and forms a subcellular network in skeletal muscle. J Cell Sci 2005; 118:673-87.
20. Sabatelli P, Lattanzi G, Ognibene A, Columbaro M, Capanni C, Merlini L, et al. Nuclear alterations in autosomal-dominant Emery-Dreifuss muscular dystrophy. Muscle Nerve 2001; 24:826-9.
21. Park YE, Hayashi YK, Goto K, Nonaka I, Noguchi S, Nishino I. Nuclear Changes in Skeletal Muscles Extend to Satellite Cells in AD-EDMD/LGMD1B. Neuromuscul Disord 2008; In Press.
22. Fidzianska A, Toniolo D, Hausmanowa-Petrusewicz I. Ultrastructural abnormality of sarcolemmal nuclei in Emery-Dreifuss muscular dystrophy (EDMD). J Neurol Sci 1998; 159:88-93.
23. Fidzianska A, Hausmanowa-Petrusewicz I. Architectural abnormalities in muscle nuclei. Ultrastructural differences between X-linked and autosomal dominant forms of EDMD. J Neurol Sci 2003; 210:47-51.
24. Fidzianska A, Bilinska ZT, Tesson F, Wagner T, Walski M, Grzybowski J, et al. Obliteration of cardiomyocyte nuclear architecture in a patient with LMNA gene mutation. J Neurol Sci 2008; 271:91-6.
25. Ozawa R, Hayashi YK, Ogawa M, Kurokawa R, Matsumoto H, Noguchi S, et al. Emerin-lacking mice show minimal motor and cardiac dysfunctions with nuclear-associated vacuoles. Am J Pathol 2006; 168:907-17.
26. Harding TM, Morano KA, Scott SV, Klionsky DJ. Isolation and characterization of yeast mutants in the cytoplasm to vacuole protein targeting pathway. J Cell Biol 1995; 131:591-602.
27. Klionsky DJ, Cregg JM, Dunn WA Jr, Emr SD, Sakai Y, Sandoval IV, et al. A unified nomenclature for yeast autophagy-related genes. Dev Cell 2003; 5:539-45.
28. Tanida I, Ueno T, Kominami E. LC3 conjugation system in mammalian autophagy. Int J Biochem Cell Biol 2004; 36:2503-18.
29. Dunn WA Jr, Cregg JM, Kiel JA, van der Klei IJ, Oku M, Sakai Y, et al. Pexophagy: the selective autophagy of peroxisomes. Autophagy 2005; 1:75-83.
30. Kim I, Rodriguez-Enriquez S, Lemasters JJ. Selective degradation of mitochondria by mitophagy. Arch Biochem Biophys 2007; 462:245-53.
31. Bernales S, Schuck S, Walter P. ER-phagy: selective autophagy of the endoplasmic reticulum. Autophagy 2007; 3:285-7.
32. Muchir A, van Engelen BG, Lammens M, Mislow JM, McNally E, Schwartz K, Bonne G. Nuclear envelope alterations in fibroblasts from LGMD1B patients carrying nonsense Y259X heterozygous or homozygous mutation in lamin A/C gene. Exp Cell Res 2003; 291:352-62.
33. Muchir A, Medioni J, Laluc M, Massart C, Arimura T, van der Kooi AJ, et al. Nuclear envelope alterations in fibroblasts from patients with muscular dystrophy, cardiomyopathy and partial lipodystrophy carrying lamin A/C gene mutations. Muscle Nerve 2004; 30:444-50.
34. Kabeya Y, Mizushima N, Ueno T, Yamamoto A, Kirisako T, Noda T, et al. LC3, a mammalian homologue of yeast Apg8p, is localized in autophagosome membranes after processing. EMBO J 2000; 19:5720-8.
35. Mizushima N, Yamamoto A, Matsui M, Yoshimori T, Ohsumi Y. In vivo analysis of autophagy in response to nutrient starvation using transgenic mice expressing a fluorescent autophagosome marker. Mol Biol Cell 2004; 15:1101-11.
36. Xie Z, Klionsky DJ. Autophagosome formation: core machinery and adaptations. Nat Cell Biol 2007; 9:1102-9.
37. Young AR, Chan EY, Hu XW, Kochl R, Crawshaw SG, High S, et al. Starvation and ULK1-dependent cycling of mammalian Atg9 between the TGN and endosomes. J Cell Sci 2006; 119:3888-900.
38. Gutierrez MG, Munafo DB, Beron W, Colombo MI. Rab7 is required for the normal progression of the autophagic pathway in mammalian cells. J Cell Sci 2004; 117:2687-97.
39. Fillingham J, Keogh MC, Krogan NJ. GammaH2AX and its role in DNA double-strand break repair. Biochem Cell Biol 2006; 84:568-77.
40. Tanida I, Minematsu-Ikeguchi N, Ueno T, Kominami E. Lysosomal turnover, but not a cellular level, of endogenous LC3 is a marker for autophagy. Autophagy 2005; 1:84-91.
41. Nakagawa I, Amano A, Mizushima N, Yamamoto A, Yamaguchi H, Kamimoto T, et al. Autophagy defends cells against invading group A Streptococcus. Science 2004; 306:1037-40.
42. Kvam E, Goldfarb DS. Nucleus-vacuole junctions and piecemeal microautophagy of the nucleus in *S. cerevisiae*. Autophagy 2007; 3:85-92.
43. Kvam E, Goldfarb DS. Nucleus-vacuole junctions in yeast: anatomy of a membrane contact site. Biochem Soc Trans 2006; 34:340-2.
44. Krick R, Muehe Y, Prick T, Bremer S, Schlotterhose P, Eskelinen EL, et al. Piecemeal microautophagy of the nucleus requires the core macroautophagy genes. Mol Biol Cell 2008; 19:4492-505.
45. Marino G, Ugalde AP, Salvador-Montoliu N, Varela I, Quiros PM, Cadinanos J, et al. Premature aging in mice activates a systemic metabolic response involving autophagy induction. Hum Mol Genet 2008; 17:2196-211.
46. Pendas AM, Zhou Z, Cadinanos J, Freije JM, Wang J, Hultenby K, et al. Defective prelamin A processing and muscular and adipocyte alterations in Zmpste24 metalloproteinase-deficient mice. Nat Genet 2002; 31:94-9.
47. Arimura T, Helbling-Leclerc A, Massart C, Varnous S, Niel F, Lacene E, et al. Mouse model carrying H222P-Lmna mutation develops muscular dystrophy and dilated cardiomyopathy similar to human striated muscle laminopathies. Hum Mol Genet 2005; 14:155-69.
48. Sullivan T, Escalante-Alcalde D, Bhatt H, Anver M, Bhat N, Nagashima K, et al. Loss of A-type lamin expression compromises nuclear envelope integrity leading to muscular dystrophy. J Cell Biol 1999; 147:913-20.
49. Carra S, Seguin SJ, Lambert H, Landry J. HspB8 chaperone activity toward poly(Q)-containing proteins depends on its association with Bag3, a stimulator of macroautophagy. J Biol Chem 2008; 283:1437-44.

Human *PTRF* mutations cause secondary deficiency of caveolins resulting in muscular dystrophy with generalized lipodystrophy

Yukiko K. Hayashi,[1] Chie Matsuda,[2] Megumu Ogawa,[1] Kanako Goto,[1] Kayo Tominaga,[1] Satomi Mitsuhashi,[1] Young-Eun Park,[1] Ikuya Nonaka,[1] Naomi Hino-Fukuyo,[3] Kazuhiro Haginoya,[3,4] Hisashi Sugano,[5] and Ichizo Nishino[1]

[1]Department of Neuromuscular Research, National Institute of Neuroscience, National Center of Neurology and Psychiatry, Kodaira, Tokyo, Japan. [2]Neuroscience Research Institute, National Institute of Advanced Industrial Science and Technology, Tsukuba, Ibaraki, Japan. [3]Department of Pediatrics, Tohoku University School of Medicine, Sendai, Miyagi, Japan. [4]Department of Pediatric Neurology, Takuto Rehabilitation Center for Children, Sendai, Miyagi, Japan. [5]Department of Metabolic and Endocrine Medicine, Kochi Health Science Center, Kochi, Kochi, Japan.

Caveolae are invaginations of the plasma membrane involved in many cellular processes, including clathrin-independent endocytosis, cholesterol transport, and signal transduction. They are characterized by the presence of caveolin proteins. Mutations that cause deficiency in caveolin-3, which is expressed exclusively in skeletal and cardiac muscle, have been linked to muscular dystrophy. Polymerase I and transcript release factor (PTRF; also known as cavin) is a caveolar-associated protein suggested to play an essential role in the formation of caveolae and the stabilization of caveolins. Here, we identified *PTRF* mutations in 5 nonconsanguineous patients who presented with both generalized lipodystrophy and muscular dystrophy. Muscle hypertrophy, muscle mounding, mild metabolic complications, and elevated serum creatine kinase levels were observed in these patients. Skeletal muscle biopsies revealed chronic dystrophic changes, deficiency and mislocalization of all 3 caveolin family members, and reduction of caveolae structure. We generated expression constructs recapitulating the human mutations; upon overexpression in myoblasts, these mutations resulted in PTRF mislocalization and disrupted physical interaction with caveolins. Our data confirm that PTRF is essential for formation of caveolae and proper localization of caveolins in human cells and suggest that clinical features observed in the patients with *PTRF* mutations are associated with a secondary deficiency of caveolins.

Introduction

Caveolae are specific invaginations of the plasma membrane characterized by the presence of the protein caveolin. To date, 3 caveolin family members have been identified. Caveolin-1 and -2 are coexpressed in many cell types, such as endothelial cells, smooth muscle cells, fibroblasts, and adipocytes, and form a hetero-oligomeric complex (1). In contrast, caveolin-3 is expressed exclusively in skeletal and cardiac muscles (2). Caveolae are involved in several important cellular processes, including clathrin-independent endocytosis, regulation and transport of cellular cholesterol, and signal transduction (3, 4).

Polymerase I and transcript release factor (PTRF; also known as cavin) is a highly abundant caveolae component and is suggested to have an essential role in caveolar formation. In both mammalian cells and zebrafish, knockdown of PTRF leads to a reduction in caveolae density (5). Mice lacking PTRF do not have morphologically detectable caveolae, in addition to a markedly diminished protein expression of all 3 caveolin isoforms (6). Interestingly, PTRF-knockout mice mimic lipodystrophy in humans, demonstrating considerably reduced adipose tissue mass, high circulating triglyceride levels, glucose intolerance, and hyperinsulinemia (6).

Here we report that mutations in *PTRF* (GenBank accession no. 284119) caused a disorder presenting as generalized lipodystrophy and muscular dystrophy. We demonstrate that this condition was associated with deficiency and mislocalization of all 3 caveolin family members and reduction of caveolae structure.

Conflict of interest: The authors have declared that no conflict of interest exists.

Citation for this article: *J. Clin. Invest.* **119**:2623–2633 (2009). doi:10.1172/JCI38660.

Results

Identification of PTRF mutations. Deficiency of caveolin-3 as a result of *CAV3* gene mutations is known to cause muscular dystrophy (7). We found 5 nonconsanguineous Japanese patients whose muscle showed caveolin-3 deficiency but without *CAV3* mutation among 2,745 muscular dystrophy specimens kept in the muscle repository of the National Center of Neurology and Psychiatry. Importantly, all 5 patients also had congenital generalized lipodystrophy (CGL; also known as Berardinelli-Seip syndrome). From the findings observed in lacking cells and animal models lacking PTRF (5, 6), we screened for *PTRF* mutations.

We identified 2 different frameshift mutations in all 5 patients examined: patients 1–4 (P1–P4) had the same homozygous c.696_697insC (p.K233fs) mutation in exon 2, and P5 harbored a compound heterozygous mutation of the same c.696_697insC and c.525delG (p.E176fs) in exon 2 (Figure 1A). The c.525delG mutation changes the last 275 amino acids to an unrelated 98-amino acid sequence, whereas c.696_697insC substitutes the last 158 amino acids with an unrelated 191-amino acid sequence (Figure 1B). Both mutations were not identified in the chromosomes of 200 Japanese control subjects.

In order to determine whether the common c.696_697insC mutation has the same haplotype, we examined 6 sets of single nucleotide polymorphisms (SNPs) within *PTRF*: rs2062213, rs8070945, rs963988, rs963987, rs963986, and rs9252. All 5 patients had the same haplotype for all 6 SNPs, which occurred homozygously (Table 1). During mutation screening, we found a novel 9-bp insertion polymorphism in the 3′ noncoding region

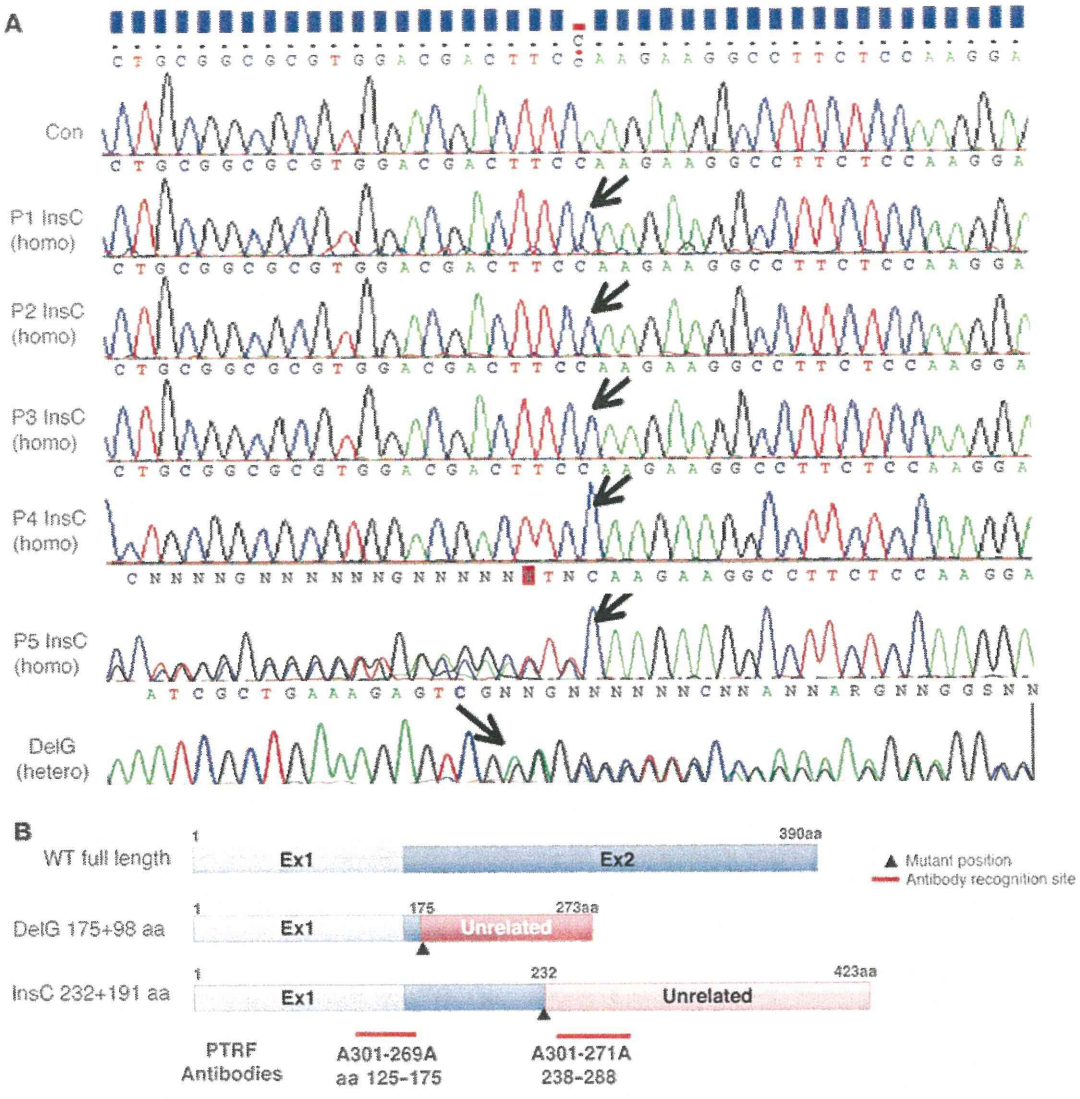

Figure 1

Mutations in *PTRF*. (**A**) All 5 patients had a homozygous or compound heterozygous mutation in *PTRF* (shown by arrows). P1–P4 had the same homozygous insertion mutation of c.696_697insC (InsC) in exon 2, whereas P5 had a compound heterozygous mutation of the same c.696_697insC insertion mutation and a deletion mutation of c.525delG (DelG) in exon 2. (**B**) Schema of the position of mutations in *PTRF*, putative proteins produced by mutations, and antibody recognition sites. The c.525delG mutant changes the last 275 amino acids to an unrelated 98–amino acid sequence, while the c.696_697insC mutant substitutes the last 158 amino acids with an unrelated 191–amino acid sequence.

of *PTRF* (c.1235_1236insTCTCGGCTC). This 9-bp insertion was found heterozygously in 26% and homozygously in 2% of Japanese control individuals. In P1–P5, none had this 9-bp insertion. We also examined 2 microsatellite markers (STS-W93348 and D17S1185) close to *PTRF* and found heterozygosity in the patients (Table 1). From these results, a founder effect may not be likely, although we could not completely rule out the possibility.

Mutation screening of the other genes associated with lipodystrophy and muscular dystrophy. From the clinical and pathological findings, we performed mutation screening for the genes associated with muscular dystrophy and lipodystrophy, including *CAV3*, *LMNA*, *AGPAT2*, *BSCL2*, *CAV1*, *PPARG*, *AKT2*, and *ZMPSTE24*. We found a heterozygous nucleotide change of c.1138G>A (p.D380N) in *BSCL2* in P1. This substitution was also identified heterozygously in 16% of Japanese control individuals, and we believe this to be a novel nonsynonymous SNP. For all the other genes examined, no other mutation was identified in P1–P5.

Clinical features of the patients with PTRF mutations. Clinical information for P1–P5 is summarized in Table 2. Common to all patients was the presence of muscular dystrophy and generalized lipodystrophy. However, despite having the same mutation, the patients' additional symptoms were variable. Generalized loss of subcutaneous adipose tissue in several areas, including the face, was noticed in infancy or early childhood. Hepatosplenomegaly, acromegaloid features, and umbilical prominence were often observed in the patients. No patient showed intellectual deficit or acanthosis nigricans. Patients presented with mild muscle weakness, but with hypertrophy of muscles (Figure 2A). Electrically silent percussion-induced

Table 1
Haplotype analysis

	P1	P2	P3	P4	P5	Control[A]
Intron 1, rs2062213	C/C	C/C	C/C	C/C	C/C	C/C (53%)
Intron 1, rs8070945	C/C	C/C	C/C	C/C	C/C	C/C (78%)
Intron 1, rs963988	G/G	G/G	G/G	G/G	G/G	G/G (33%)
Intron 1, rs963987	G/G	G/G	G/G	G/G	G/G	G/G (31%)
Intron 1, rs963986	G/G	G/G	G/G	G/G	G/G	G/G (34%)
Exon 2, 9-bp insertion[B]	no/no	no/no	no/no	no/no	no/no	no/no (72%)
Exon 2, rs9252[B]	C/C	C/C	C/C	C/C	C/C	C/C (78%)
STS-W93348 (bp)	251/253	251/253	251/253	251/253	251/253	251/253/264
D17S1185 (bp)	219/219	170/219	170/219	170/170	170/203	170/203/215/219/225/237

[A]Percentages denote the frequency of the haplotype in the HapMap JPT population. [B]Exon 2 is 3′ noncoding.

muscle mounding was characteristic. Cardiac arrhythmia, transient immunodeficiency, recurrent pneumonia, constipation, and chalasia were variably seen. Available laboratory data in the patients are summarized in Table 3. Metabolic complication was mild, and none of our patients showed marked elevation of fasting glucose levels. The result of oral glucose tolerance tests revealed moderate fasting hyperinsulinemia in P1 and P2 associated with glucose intolerance in P2, but normal levels in P4 (Table 4). High triglyceremia was seen in P4 and P5. Serum creatine kinase (CK) levels were moderately elevated in all patients. Abdominal CT images of P4 revealed marked loss of subcutaneous and intra-abdominal fat (Figure 2, B and C). In addition, his body fat ratio, as determined by whole body dual energy X-ray absorptiometry, was 7.1% (Supplemental Table 1; supplemental material available online with this article; doi:10.1172/JCI38660DS1), while head fat was relatively preserved.

Clinical features of the heterozygous parents. There was no family history of muscular dystrophy or lipodystrophy in P1–P5. Genetic analysis revealed a heterozygous c.696_698insC mutation in both parents of P4. Clinically, both father and mother had hypertension requiring medication, whereas P4 was normotensive. Mild lipid metabolism abnormality and borderline glucose intolerance was also seen (Supplemental Table 2). DNA samples from the other parents were not available.

Loss of PTRF with deficiency or mislocalization of caveolins in skeletal muscle. Biopsied skeletal muscles from P1–P5 showed consistent findings, with chronic dystrophic changes including marked variation in muscle fiber size, increased number of fibers containing internalized nuclei, a few necrotic and regenerating fibers, and increased interstitial fibrosis (Figure 2D and Supplemental Figure 1). Intramuscular lipid droplets, as visualized by oil red O staining, were not increased (Figure 2D).

Immunohistochemistry demonstrated that the PTRF antibodies A301-269A and A301-271A (which recognize the N- and C-terminal regions of the protein, respectively; Figure 1B) showed sarcolemmal membrane staining of muscle fibers, with stronger immunoreaction at intramuscular blood vessels in control muscles (Figure 3A). Caveolin-3 was clearly observed at sarcolemma, whereas caveolin-1 and -2 were present only in blood vessels. In contrast, muscles from P1–P5 showed barely detectable immunoreaction to both PTRF antibodies (Figure 3A). Caveolin-3 immunoreactivity was greatly reduced in the sarcolemma, but cytoplasmic staining was remarkably increased. This caveolin-3 staining pattern was similar to that seen in the patients with muscular dystrophy

Table 2
Clinical summary

	P1	P2	P3	P4	P5
Age/sex	8-yr-old female	14-yr-old female	10-yr-old male	27-yr-old male	24-yr-old male
Height, body weight	124 cm, 21.3 kg	149 cm, 40.5 kg	NA	164 cm, 49.0 kg	152 cm, 40 kg
Lipodystrophy	Generalized	Generalized	Generalized	Generalized	Generalized
Mental retardation	No	No	No	No	No
Acanthosis nigricans	No	No	No	No	No
Liver/spleen	Hepatosplenomegaly	Fatty liver	NA	Hepatosplenomegaly	No
Endocrine abnormalities	Reduced growth hormone secretion	NA	NA	Accelerated bone age, acromegaloid features, no androgynism	Acromegaloid features, no androgynism
Muscle weakness	Distal dominant	No	No	Generalized	Distal dominant
Muscle mounding	Positive	NA	NA	Positive	Positive
Other muscle symptoms	Muscle hypertrophy	Myalgia, muscle stiffness	NA	Muscle hypertrophy	Muscle hypertrophy
Cardiac symptoms	Arrhythmia	No	No	Atrial fibrillation	No
Skeletal abnormalities	Lordosis, Contractures (ankles, shoulders, fingers)	No	No	Scoliosis, contractures (ankles)	Scoliosis
Other symptoms	Constipation	Transient IgA deficiency, recurrent pneumonia	Nephrosis	Umbilical prominence, renal stones	Recurrent pneumonia, chalasia, constipation

NA, not available.

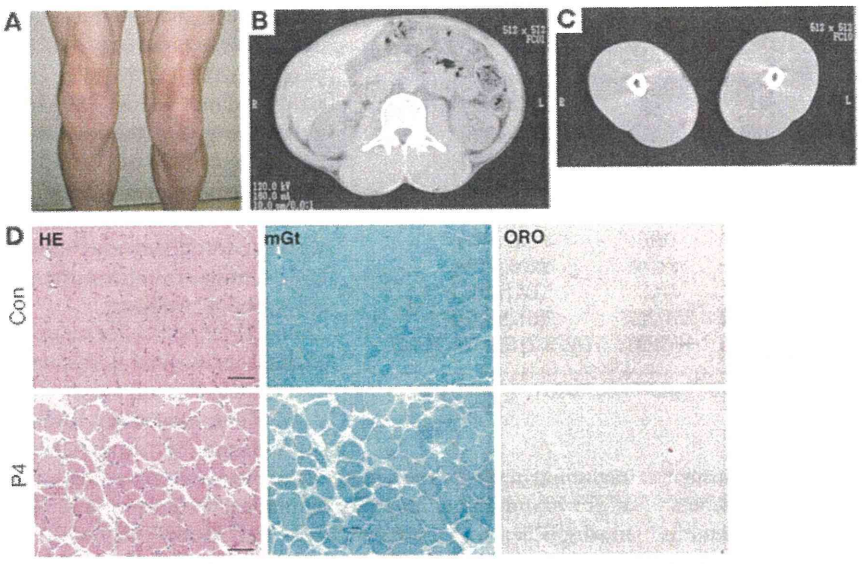

Figure 2
Muscle hypertrophy and dystrophic changes. (**A**) Prominent musculature feature of legs in P5. (**B** and **C**) CT images from P4 showed hypertrophy of paravertebral and thigh muscles with minimal subcutaneous and intra-abdominal fat tissue. (**D**) H&E stain of biopsied skeletal muscle from P4 showed dystrophic changes, including marked variation in fiber size, enlarged fibers with internalized nuclei, endomysial fibrosis, and few necrotic and regenerating fibers. Intramuscular lipid droplets were not increased compared with control. mGt, modified Gomori trichrome; ORO, oil red O. Scale bars: 50 μm.

caused by *CAV3* mutations (data not shown). Similarly, dysferlin was decreased in the sarcolemma and mislocalized into the cytoplasm (data not shown), and the same pattern is also seen in muscles of individuals with *CAV3* mutations (8). Immunoreactivity to caveolin-1 and caveolin-2 in blood vessels was barely detectable in P1–P5 (Figure 3A). Other antibodies related to muscular dystrophy, including dystrophin, sarcoglycans, dystroglycans, emerin, merosin, and collagen VI, showed normal immunostaining patterns (data not shown).

Immunoblotting showed detection of PTRF as an approximately 50-kDa band in control muscles and 3T3 cells, which were used as a positive control. No band was detected in the muscle of P1–P5 (Figure 3B). Caveolin-3 was detected in all samples examined, but relative protein amount, determined using densitometry and normalized by myosin heavy chain (MHC), decreased in P1–P5 compared with control subjects (Figure 3C). The band for caveolin-2 was observed in control muscles and 3T3 cells, but was barely detectable in the muscles of P1–P5 (Figure 3B).

In order to determine mRNA expression of PTRF, RT-PCR was performed using total RNA extracted from biopsied skeletal muscles. Using primers designed to amplify whole coding region of mRNA, PTRF was amplified as a single transcript in control muscles. In contrast, no PCR product was amplified in P1–P5 (Figure 4A). To compare mRNA levels for caveolins, we performed quantitative RT-PCR and normalized results to GAPDH expression. The mRNA amounts of all 3 caveolin families in the patients' muscles were variable, but not markedly decreased, compared with control muscles (Figure 4, B and C). Preserved mRNA levels, but decreased protein amounts of caveolins, suggested destabilization of caveolin proteins when PTRF is lacking, as previously reported (9).

Loss of PTRF causes reduced caveolae formation in human muscles. Greatly reduced caveolae formation was previously reported in PTRF knockdown mammalian cells, zebrafish, and knockout mice (5, 9). Decreased caveolae number was also reported in skeletal muscle from limb girdle muscular dystrophy type 1C (LGMD1C) patients with *CAV3* mutations (10). We therefore examined muscle caveolae in P2 and P3 using electron microscopy. Plasma membrane of muscle fibers from both patients was nearly flat, and caveolae density was notably reduced, compared with control muscle (Figure 5). Caveolae formation in the intramuscular vascular smooth muscle cells was also remarkably reduced (data not shown).

Altered localization of mutant PTRF and reduced interaction with caveolins in transfected cells. In order to determine the intracellular localization of mutant PTRF, FLAG-tagged WT or 2 mutants (c.525delG and c.696_697insC) and T7-tagged caveolin-3 or -1 were cotransfected in C2C12 myoblasts and COS-7 cells. In C2C12 cells, WT PTRF was detected at the cell membrane and colocalized with caveolin-3 (Figure 6A). Interestingly, c.525delG was detected as intranuclear aggregations and was not observed at the cell membrane (Figure 6, A and B). Caveolin-3 was present only in cytoplasm, and did not merge with PTRF (Figure 6A). The c.696_697insC mutant was observed as microtubular filament network in cytoplasm and colocalized with β-tubulin (Figure 6B). This finding is consistent with the localization of the truncated $PTRF_{1-322}$, as described previously (9). Similar mislocalization and/or aggregation of transfected mutant PTRF was observed in COS-7 cells (data not shown).

Table 3
Laboratory data

Measurement	Reference range	P1	P2	P3	P4	P5
CK (IU/l)	56–244	1,374	542–2,253	2,000	554–1,545	645–2,630
Fasting glucose (mg/dl)	70–109	75	99	NA	93–116	102
HbA1c (%)	4.3–5.8	NA	NA	NA	5.0–5.4	NA
Total cholesterol (mg/dl)	130–220	164	NA	NA	185–267	218
Triglyceride (mg/dl)	50–150	93	NA	NA	143–450	359
LDL-C (mg/dl)	70–139	NA	NA	NA	188	NA
Leptin (ng/ml)	0.9–13.0	NA	NA	NA	0.6	NA
Adiponectin (μg/ml)	None	NA	NA	NA	1.05	NA

NA, not available.

Table 4
Oral glucose tolerance test of P1, P2, and P4

	Pre	30 min	60 min	120 min
P1				
Glucose (mg/dl)	75	98	69	62
IRI (μU/ml)	22.8	141.6	64.7	23.8
P2				
Glucose (mg/dl)	99	127	160	172
IRI (μU/ml)	20	53	65	80
P4				
Glucose (mg/dl)	93	124	140	70
CPR (ng/ml)[A]	2.8	5.9	8.3	5.5
IRI (μU/ml)	1.0	22.3	32.9	6.2

IRI, immunoreactive insulin; CPR, C-peptide immunoreactivity. [A]Reference range, 0.7–2.2 ng/ml.

We performed immunoprecipitation assay in order to examine the binding ability of PTRF and caveolins. WT PTRF was coimmunoprecipitated by anti-T7 antibody, and vice versa (Figure 6, C and D). The c.525delG mutant showed smaller molecular weight (estimated 30 kDa; Figure 1B), and no immunoprecipitated protein was detected by FLAG and T7 antibodies. The c.696_697insC mutant showed slightly larger molecular weight, and coimmunoprecipitated proteins were greatly reduced (Figure 6, C and D). These results suggest that mutant PTRFs cannot localize properly and lose their binding ability to caveolins even if they are produced.

Activation of myostatin and Akt signaling pathways in PTRF-deficient skeletal muscles. Caveolin-3 is suggested to have an important role for suppression of myostatin-mediated signaling in skeletal muscle (11). In order to determine the functions of mislocalized caveolin-3 in *PTRF* mutated cells, we performed quantitative RT-PCR for myostatin and immunoblotting analysis to examine phosphorylation status of Mad homolog 2/3 (p-Smad2/3), an intracellular effector of myostatin in skeletal muscles. In P1–P5, increased amounts of p-Smad2/3$^{S423/425}$ were observed in skeletal muscles, while myostatin mRNA levels were variable (Figure 7, A–C). Positive immunoreaction to p-Smad2/3 was detected in few myonuclei from muscle of patients with *PTRF* or *CAV3* mutations, but not in those from muscle of control subjects (data not shown). These results suggest that myostatin signaling is also activated in P1–P5.

Despite the activation of myostatin, a negative regulator of muscle growth, the patients showed hypertrophy of muscles. Since Akt (also known as protein kinase B) is known as the key molecule to regulate muscle mass (12), we examined p-Akt^{T308} and p-Akt^{S473} by immunoblotting analysis. p-Akt was elevated in the muscle of P1–P5 compared with controls, except for p-Akt^{S473} in P2 (Figure 7, D–F). This result suggests that Akt pathway is activated, probably through an as-yet-unidentified mechanism, and could contribute to the muscle hypertrophy observed in P1–P5.

Neuronal NOS activity is variable and mildly increased in PTRF-deficient skeletal muscles. Caveolin-3 is known to interact with and negatively regulate the catalytic activity of neuronal NOS (nNOS) in skeletal muscle (13); this notion is supported by the finding of increased nNOS activity in muscle of transgenic mice expressing mutant caveolin-3 (14). We thus examined nNOS expression and its activity in muscles from patients with mutations in *PTRF* or *CAV3* compared with those from age-matched controls. The immunoreactivity of nNOS was seen in sarcolemma and cytoplasm of each muscle fiber with variable intensity, but no obvious difference was seen between patients and controls (Figure 3A). Immunoblotting analysis also revealed comparable amounts of nNOS (Figure 3, B and D). In order to examine nNOS activity of each muscle fiber, we performed NADPH diaphorase (NDP) activity assay. The intensity of NDP staining appeared variable among muscle fibers and was slightly increased in patients with mutations in *PTRF* or *CAV3* compared with age-matched controls (Figure 8).

Discussion

Lipodystrophy is a heterogeneous group of disorders characterized by loss of adipose tissue from the body. The degree of fat loss varies from small areas to near-complete absence of adipose tissue. The extent of fat loss usually determines clinical severity and metabolic complications, such as insulin resistance and high levels of serum triglycerides.

Several genes responsible for inherited lipodystrophy have been identified. CGL is an autosomal-recessive disorder, with most patients presenting soon after birth with severe insulin resistance and elevated serum triglycerides. CGL1 is caused by mutations in *AGPAT2* on chromosome 9q34, which encodes 1-acylglycerol-3-phospate-O-acyltransferase 2, an enzyme involved in the biosynthesis of triacylglycerol and glycerophospholipids (15). CGL2 is caused by mutations in *BSCL2* on chromosome 11q13, which encodes a functionally unknown protein named seipin (16). Recently, mutations in *CAV1* on chromosome 7q31 have been reported to cause generalized (i.e., CGL3) and partial lipodystrophy (17, 18).

Several causative genes for autosomal-dominant familial partial lipodystrophy are known: *LMNA* on chromosome 1q21 (19), *ZMPSTE24* on chromosome 1p34 (20), *AKT2* on chromosome 19q13 (21), *PPARG* on chromosome 3p25 (22), and *LMNB2* on chromosome 19q1 (23). Nevertheless, many patients clinically diagnosed with lipodystrophy carry no mutation in the known genes, suggesting the presence of other causative genes.

Here we conclude that *PTRF* mutations can cause CGL. In our series, patients showed generalized loss of adipose tissue from infancy or early childhood. Because PTRF is reported to colocalize with hormone-sensitive lipase and translocate to the nucleus in the presence of insulin in adipocytes (24), it could be surmised that PTRF plays an important role in lipid metabolism and insulin-regulated gene expression. Interestingly, metabolic complications were milder in patients with *PTRF* mutations than in patients with CGL1 and CGL2, and these were observed only in the elder patients. Although we could not examine the status of caveolae and caveolins in adipose tissues, the secondary deficiency of caveolins might have an important role in the process of lipodystrophy, since *CAV1* mutation can cause lipodystrophy in both humans and mice (17, 18, 25). Notably, the heterozygous parents had mild metabolic disorders, but a robust conclusion could not be reached, as a limited number of the heterozygous carriers of the *PTRF* mutation were available to us. Further investigation is needed to determine the effect of haploinsufficiency of PTRF.

Skeletal muscle symptoms with serum CK elevation represent another common symptom in patients with *PTRF* mutations. The clinical and pathological findings are very similar to those observed in patients with *CAV3* mutation (7, 26–28), although P1–P5 had no *CAV3* mutations. The secondary loss of caveolin-3 in the sarcolemma may contribute to the muscle phenotype. Moreover, serum CK elevation may be a good laboratory marker for diagnosis of lipodystrophy patients with *PTRF* mutations.

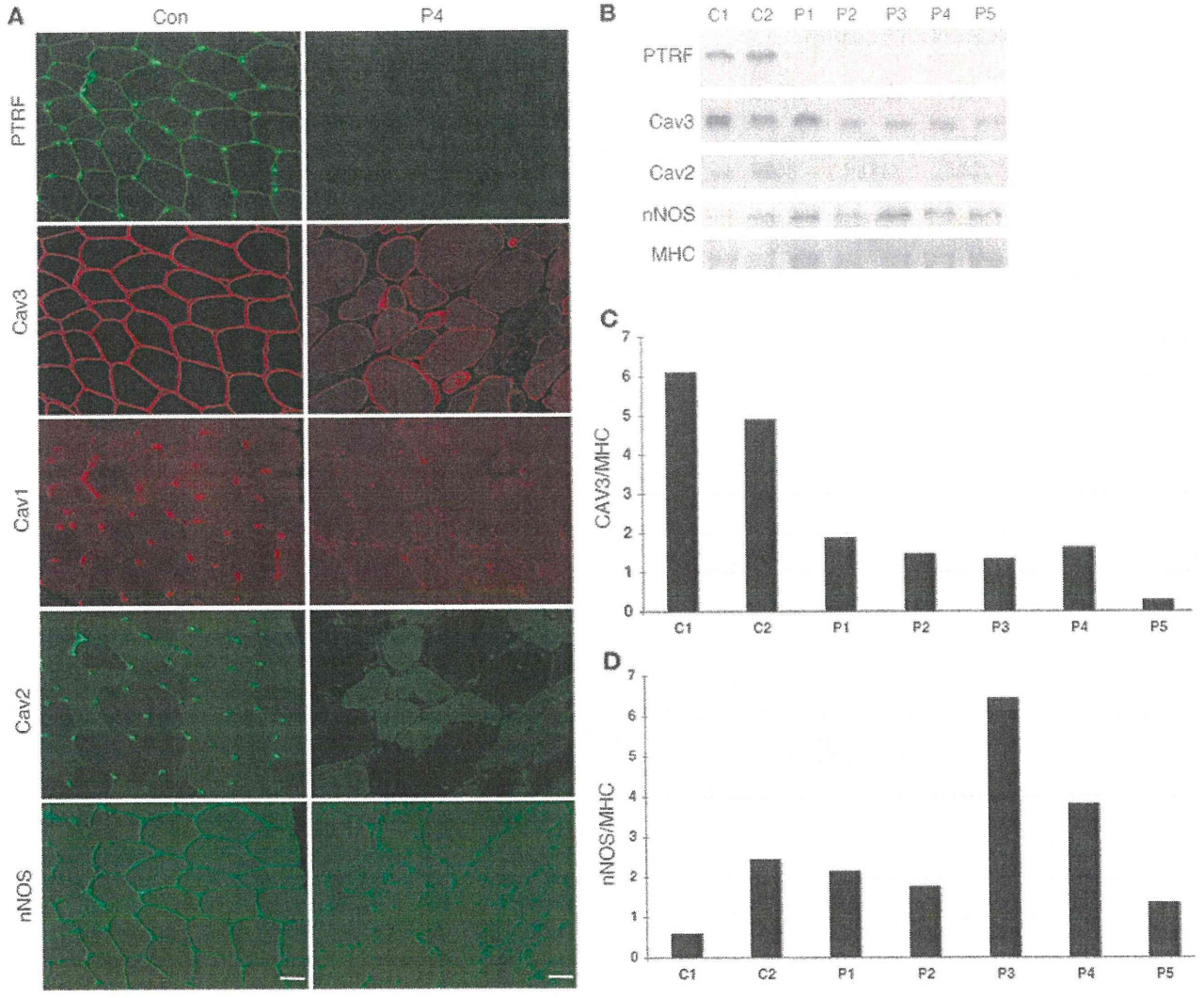

Figure 3

Loss of PTRF is associated with deficiency and mislocalization of caveolins in muscle. (**A**) In control muscle, PTRF was clearly seen in sarcolemma as strongly staining blood vessels. Caveolin-3 (Cav3) was clearly visible at sarcolemma, and caveion-1 and -2 stained intramuscular blood vessels. The muscle of P4 was negative for PTRF. Membrane staining of caveolin-3 was reduced with increased cytoplasmic staining, and caveolin-1 and -2 were barely detectable. Immunoreactivity of nNOS varied between muscle fibers, but was not markedly different between control and patient muscle. Scale bar: 50 μm. (**B**) Immunoblotting analysis of skeletal muscles. 3T3 cells were used as a positive control. PTRF and caveolin-2 were seen only in the muscles of 2 control subjects and in 3T3 cells, and were barely detectable in the muscles of P1–P5. The bands for caveolin-3 and nNOS were variably seen. (**C** and **D**) Quantification of immunoreactive bands was performed by densitometric analysis and normalized with MHC. In P1–P5, relative amounts of caveolin-3 decreased compared with control subjects (**C**), whereas nNOS amounts varied (**D**).

Caveolin-3 was previously reported to have an important role in inhibition of myostatin signaling by suppressing activation of its type I receptor. In mutant *Cav3* transgenic mice, loss of caveolin-3 causes muscular atrophy with increased p-Smad2, and this muscle atrophy can be rescued by myostatin inhibition (11). Consistent with the secondary reduction of caveolin-3, skeletal muscles from P1–P5 showed increased amounts of p-Smad2/3. Unexpectedly, however, muscle hypertrophy was seen in these patients.

The Akt pathway, when activated, is known to promote protein synthesis, stimulate muscle hypertrophy, and inhibit atrophy-related gene expression by phosphorylating FoxO transcription factors (12). This pathway is also known to play a pivotal role in the regulation of glucose transport and glycogen synthesis in skeletal muscle cells. Akt is activated by insulin, various growth factors, nutrients, and exercise, whereas it is negatively regulated by myostatin and cytokines. Akt is phosphorylated at T308 by phosphoinositide-dependent kinase and at S473 by mammalian target of rapamycin in association with rictor. The increase in phosphorylated Akt in the muscle of P1–P5 may explain, at least in part, the muscle hypertrophy observed. Akt pathway activation might be associated with the metabolic complications observed in P1–P5. However, the upregulation of myostatin observed is contradictory to the established knowledge on muscle hypertrophy. This would be worthwhile to investigate in future studies, in order to

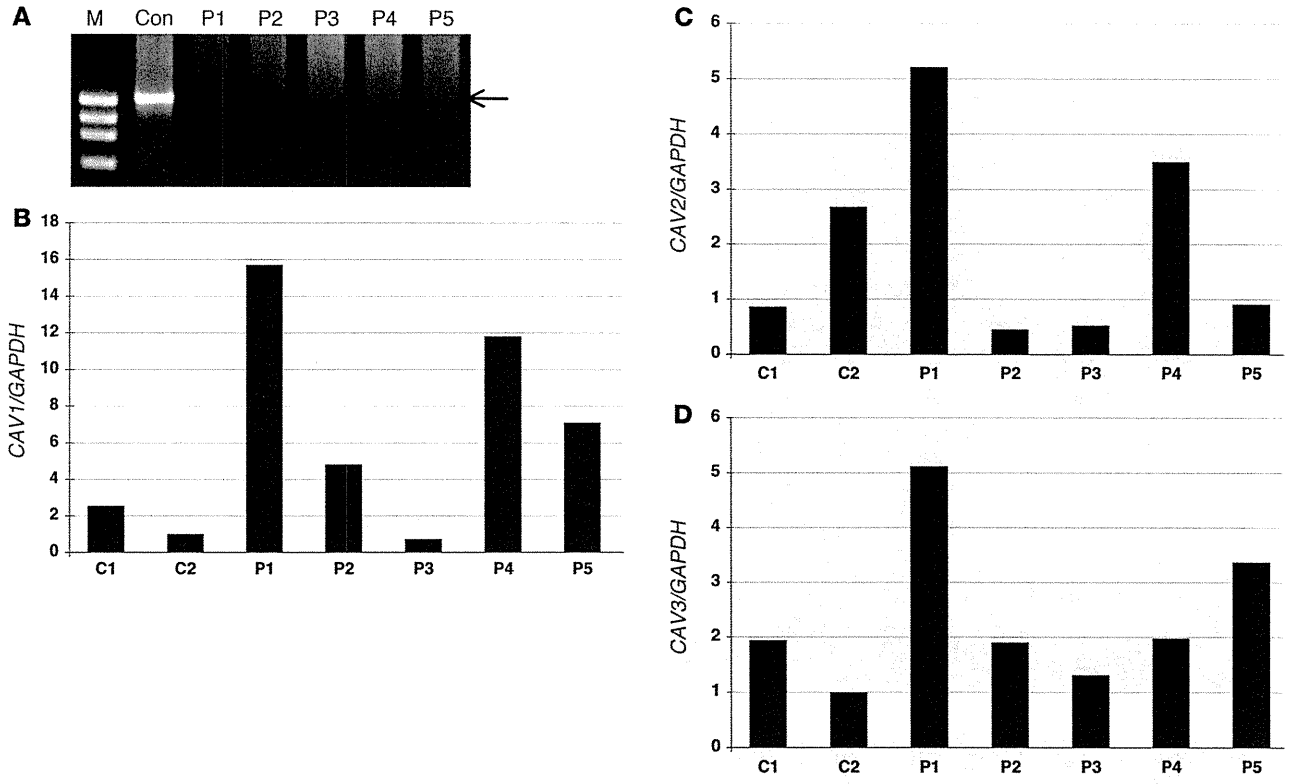

Figure 4
mRNA expression of PTRF in skeletal muscle, and quantitative RT-PCR of mRNAs for caveolins. (**A**) RT-PCR analysis revealed a single band for *PTRF* mRNA (arrow) in a control subject, but no detectable product was seen in P1–P5. M, marker. (**B–D**) By quantitative RT-PCR, mRNA for *CAV1*, *CAV2*, and *CAV3* normalized with *GAPDH* expression was not decreased in P1–P5.

elucidate the role of PTRF deficiency in muscle hypertrophy and related signaling pathway.

In addition to lipodystrophy and muscular dystrophy, P1–P5 had various other symptoms, whose association to *PTRF* mutation might be difficult to ascertain at this time. For example, 2 of 5 patients had arrhythmia. Although we could not examine the expression of caveolins in cardiac muscle, this cardiac abnormality may be caused by secondary deficiency of caveolins in heart, as cardiac involvement was previously reported in patients with *CAV3* mutations and in mutant mice with double knockout of *Cav1* and *Cav3* (29–33).

Remarkable reduction in expression of caveolin-1 and -2 with decreased caveolae density was observed in vascular endothelial cells in P1–P5. There was no obvious symptom related to vascular endothelial blood vessels in the patients; however, further careful investigation is necessary in order to determine the involvement of endothelial cells, which was observed in *Cav1* knockout mice (34). The severe constipation and esophageal dilatation observed in the patients might be associated with dysfunction of caveolin-1 in smooth muscle cells, as *Cav1* knockout mice had alteration of smooth muscles and interstitial cells of Cajal, the pacemaker cells of the muscle layers of the gastrointestinal tract (35).

Caveolae was previously suggested to have a role in the internalization of growth hormone in vitro (36). The acromegaloid features, accelerated bone age, or abnormal growth hormone activity observed in 3 patients in the present study might be associated with reduced caveolae formation. Recurrent pneumonia and transient immunodeficiency observed in 2 patients were also noted, although the pathomechanisms are still unknown. Further detailed studies are needed to elucidate the roles of PTRF; however,

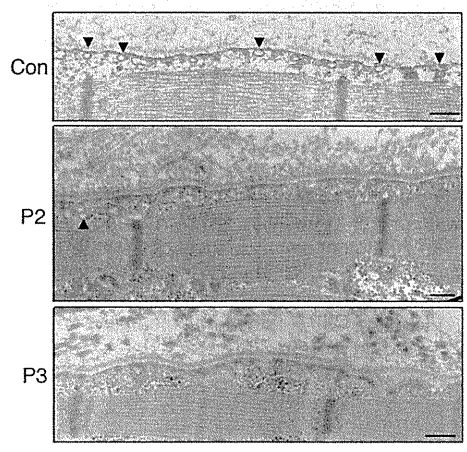

Figure 5
Reduced caveolae formation in skeletal muscle, as assessed by electron microscopy. In control muscle, an abundance of caveolae (arrowheads) was observed close to the plasma membrane. Plasma membrane of muscle fibers from P2 and P3 was nearly flat, and caveolae density was greatly reduced compared with that of control muscle. Only a few caveolae were seen in P2. Scale bars: 200 nm.

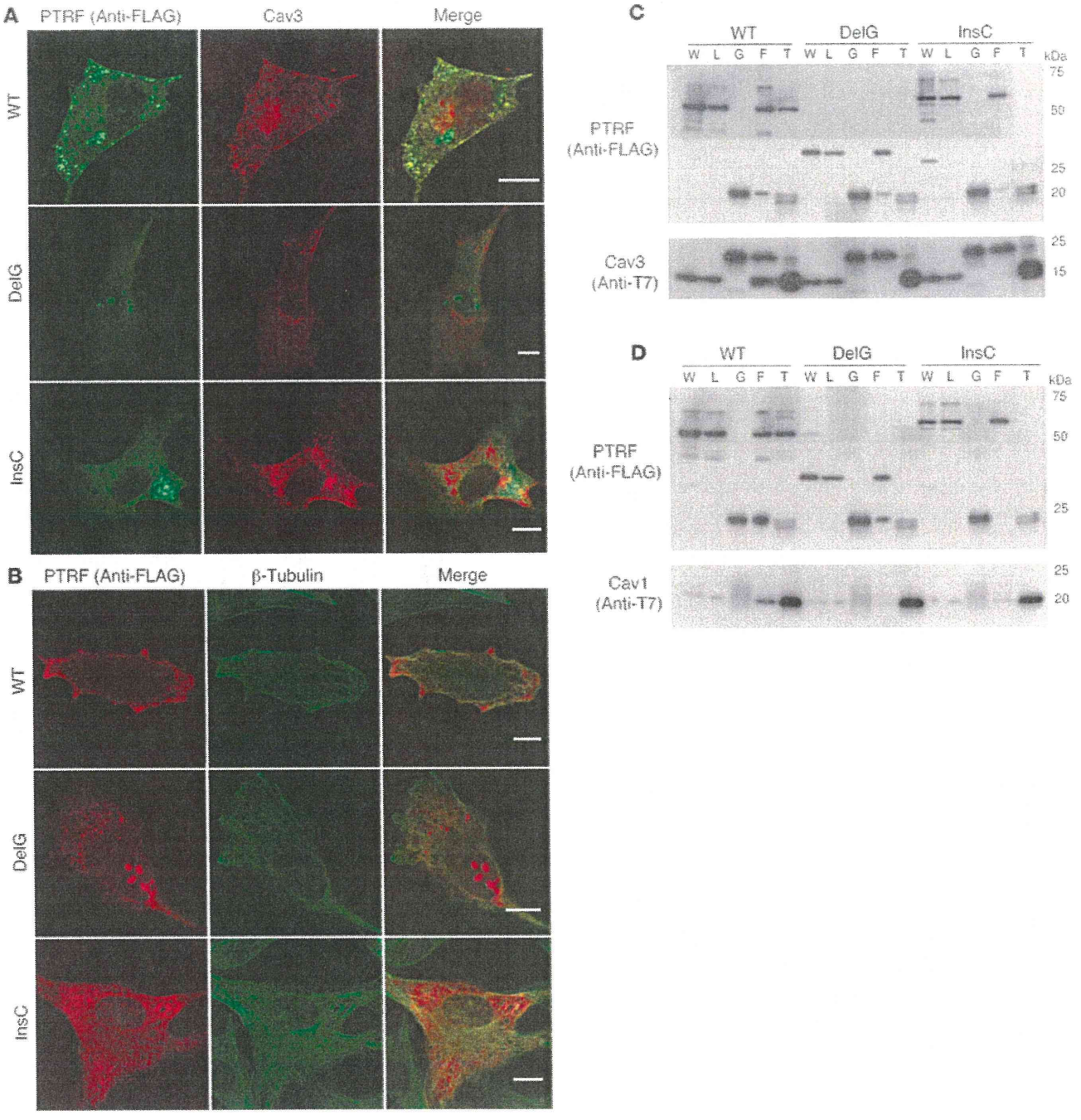

Figure 6

Altered localization of mutant PTRF in C2C12 cells and reduced binding ability to caveolins. C2C12 myoblasts were cotransfected with FLAG-tagged WT or mutant (c.525delG or c.696_697insC) PTRF cDNA and T7-tagged human caveolin-3. (**A** and **B**) WT PTRF stained by anti-FLAG antibody colocalized with caveolin-3 at the cell membrane. The deletion mutant accumulated in the nucleus, and the insertion mutant was seen in cytoplasm. (**A**) Membrane staining of caveolin-3 was decreased and was not colocalized with mutant PTRF. (**B**) The PTRF insertion mutant clearly colocalized with β-tubulin. Scale bars: 10 μm. (**C** and **D**) COS-7 cells were cotransfected with FLAG-tagged WT or mutant PTRF cDNA and T7-tagged human caveolin-3 (**C**) or caveolin-1 (**D**). The PTRF deletion mutant showed smaller molecular weight (estimated 30 kDa), and no immunoprecipitated protein was detected for FLAG or T7 antibodies. The PTRF insertion mutant showed slightly larger molecular weight, and amounts of coimmunoprecipitated proteins were greatly reduced. W, whole homogenate; L, cell lysate; G, control IgG; F, anti-FLAG; T, anti-T7.

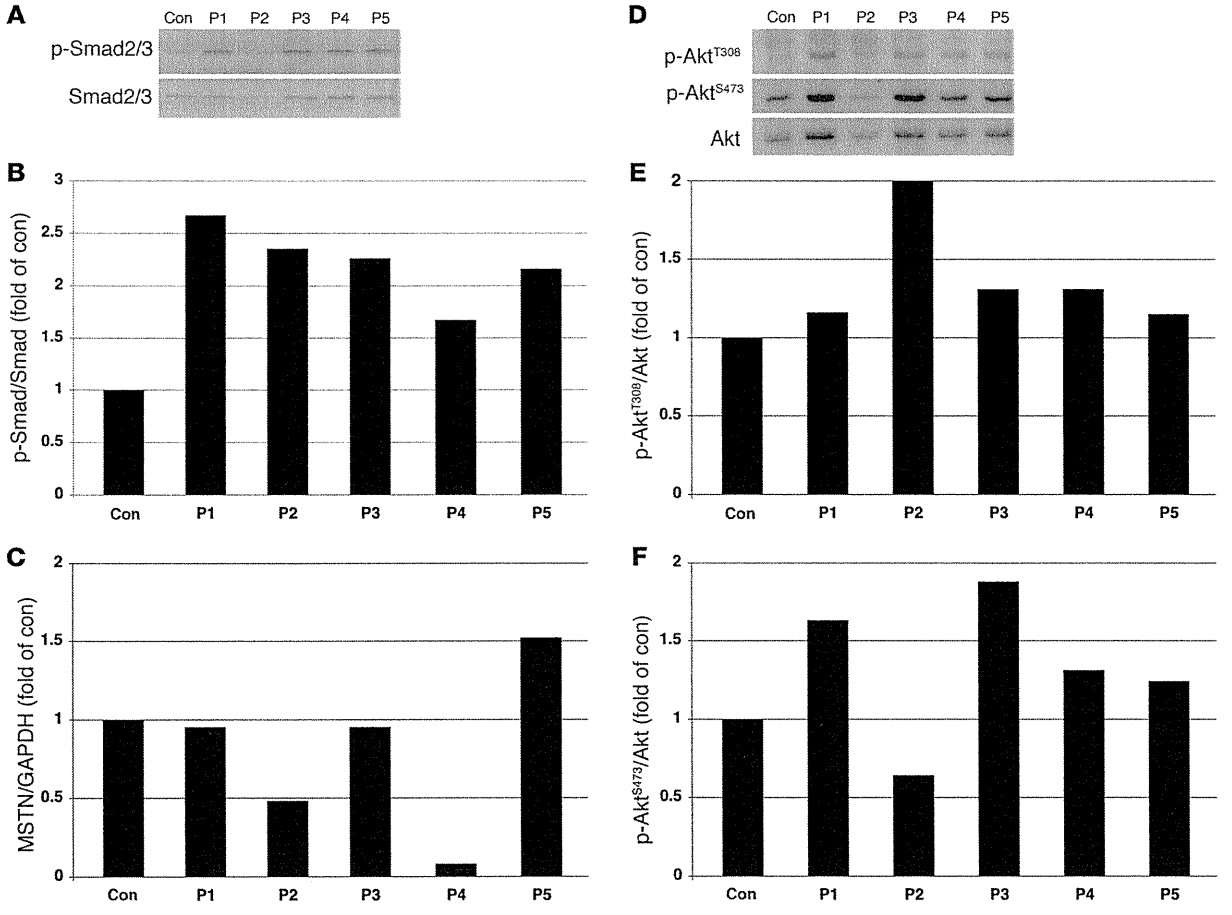

Figure 7
Increased p-Smad2 and p-Akt in P1–P5 skeletal muscle. (**A–C**) Immunoblotting analysis of Smad2/3 and p-Smad2/3$^{S423/425}$ (**A**) and densitometric analysis (**B**) showed increased p-Smad2/3 in P1–P5 compared with control muscle, with variable mRNA expression levels of myostatin (MSTN; **C**). (**D–F**) Immunoblotting analysis of p-Akt^{T308} and p-Akt^{S473}. Total Akt (**D**) and densitometric analysis (**E** and **F**) showed increased amounts of p-Akt in all patients except for p-Akt^{S473} in P2.

most clinical features observed in P1–P5 are likely to be explained by secondary reduction of caveolae and deficiency of caveolins.

Previously, Rajab et al. reported 10 of 17 patients with congenital generalized lipodystrophy unlinked to the loci of known CGL genes (37). The patients showed reduced exercise tolerance, percussion myoedema, cardiac hypertrophy, and arrhythmias. None of these patients had insulin resistance or early endocrine abnormalities (37). Ghanem also reported myoedema in a patient with Berardinelli-Seip lipodystrophy (38). Very recently, Simha et al. described CGL patients with muscle weakness and cervical spine instability (39). Because muscle involvement of these patients is similar to that of P1–P5 in the present study, *PTRF* mutations may not be rare in CGL patients.

This entity of generalized lipodystrophy with muscular dystrophy — which we believe to be novel — seems to represent a complicated disorder, as the occurrence of other symptoms could not readily be explained. Collection of detailed clinical information would therefore be essential in order to understand the precise function of PTRF.

Methods

Clinical materials. All clinical materials used in this study were obtained for diagnostic purposes and with informed consent. Subjects were selected from 2,745 muscular dystrophy specimens kept in the muscle repository of the National Center of Neurology and Psychiatry. The present studies were approved by the Ethical Committee at National Center of Neurology and Psychiatry.

Mutation screening and haplotype analysis. Genomic DNA was isolated from peripheral lymphocytes or muscles using standard techniques. All exons and their flanking intronic regions of *PTRF*, *CAV3*, *LMNA*, *AGPAT2*, *BSCL2*, *CAV1*, *PPARG*, *AKT2*, and *ZMPSTE24* were directly sequenced using genomic DNA from all patients using an ABI PRISM 3100 automated sequencer (Applied Biosystems). Primer sequences are listed in Supplemental Table 3. To confirm the compound heterozygosity in P5, the PCR product was cloned and sequenced. In order to determine the frequency of the mutations in *PTRF*, we performed enzyme digestion of PCR products from 200 Japanese control subjects using *Hpy*188III (New England Biolabs) for c.696_697insC and *Taq*I (New England Biolabs) for c.525delG. *Mbo*II (New England Biolabs) was used for enzyme digestion of PCR products to detect the c.1138G>A substitution in *BSCL2*.

For haplotype analysis, we used 6 SNPs (rs2062213, rs8070945, rs963988, rs963987, rs963986, and rs9252) within *PTRF*. PCR products were analyzed by direct sequencing or enzyme digestion using *Mae*III (Boehringer Mannheim). We also identified a novel 9-bp insertion polymorphism at the

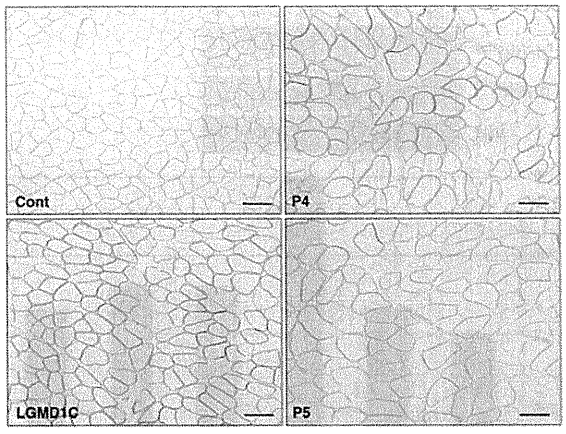

Figure 8
NDP activity assay. NDP activity was variable between muscle fibers, and was slightly increased in the muscle of P4, P5, and a LGMD1C patient with *CAV3* mutation compared with an age-matched control subject. Scale bars: 100 μm.

3′ noncoding region, and its frequency was calculated by PCR amplification using 50 Japanese control individuals. We also examined 2 microsatellite markers, STS-W93348 and D17S1185, the closest markers to *PTRF*. PCR product size was analyzed by GeneMapper using ABI 310 automated sequencer (Applied Biosystems).

Histochemical analysis. Biopsied muscle specimens were flash frozen with isopentane cooled in liquid nitrogen. Serial 10-μm-thick frozen sections were analyzed with 20 kinds of histochemical staining, including H&E, modified Gomori trichrome, NADH-tetrazolium reductase, and oil red O. The NDP activity assay was performed to examine nNOS activity of each muscle fiber, as described previously (40). In brief, 10-μm-thick frozen sections were fixed with 4% paraformaldehyde in PBS for 2 hours at 4°C. After a brief rinse with PBS, sections were incubated with 0.2% Triton X-100 in PBS for 20 minutes at 37°C. The reaction was performed for 1 hour in a dark, humidified chamber at 37°C in 0.2% Triton X-100, 0.2 mM NADPH, and 0.16 mg/ml nitro blue tetrazolium. The reaction was terminated by washing with water. We examined 6 age-matched controls and 2 LGMD1C patients with *CAV3* mutations (p.R27G and p.E33K).

Immunohistochemical analysis. Immunostaining was performed using standard methods. Serial 6-μm-thick frozen muscle sections were fixed in cold acetone for 5 minutes. After blocking with normal goat serum, sections were incubated with the primary antibodies for 2 hours at 37°C. We used antibodies against PTRF (A301-269A and A301-271A; BETHYL Laboratories), caveolin-1 (BD Biosciences), caveolin-2 (Sigma-Aldrich), caveolin-3 (BD Biosciences), and nNOS (BD Biosciences). Rabbit anti-PTRF antibody of A301-269A recognizes residue from 125 to 175, and A301-271A was raised against residue 238 and 288 of human PTRF (Figure 1B). In order to exclude other diagnosable muscular dystrophies, we used antibodies for dystrophin (DYS1, DYS2, and DYS3; Novocastra); α-, β-, γ-, and δ-sarcoglycans (Novocastra); α-dystroglycan (Upstate Biotech); β-dystroglycan (Novocastra); dysferlin (Novocastra); emerin (Novocastra); merosin (Chemicon); and collagen VI (ICN Biomedicals). After 6 rinses with PBS, sections were incubated with secondary antibodies of Alexa Fluor 488– or Alexa Fluor 568–labeled goat anti-mouse or -rabbit antibodies at room temperature for 45 minutes.

Immunoblotting analysis. Immunoblotting analysis was performed according to standard methods. Frozen muscle specimens were homogenized in SDS sample buffer and centrifuged at 15,000 *g* for 5 minutes. Protein (20 μg) from each sample was loaded on 12% SDS-polyacrylamide gels and transferred to PVDF membranes (Millipore). The membranes were blocked with 5% skim milk in PBS and immunoreacted with antibodies to PTRF (A301-269A and A301-271A), caveolin-2, caveolin-3, nNOS, Smad2/3 (Cell Signaling Technology), p-Smad2/3$^{S423/425}$ (Santa Cruz Biotechnology Inc.), Akt (Cell Signaling Technology), p-Akt^{T308} (Cell Signaling Technology), and p-Akt^{S473} (Cell Signaling Technology) overnight at 4°C. After washing in PBS containing 0.1% Tween-20, the membrane was incubated with horseradish peroxidase–labeled secondary antibody and visualized with ECL (Amersham Pharmacia Biotech). Data were analyzed using LAS-1000 chemiluminescence imaging system (Fujifilm). Quantification of immunoreactive bands was performed by densitometric analysis using Quantity One (PDI), and protein amounts for caveolin-3 and nNOS were normalized by the intensity of MHC. The ratio of p-Smad2/3 and p-Akt, to Smad and Akt, respectively, was also calculated.

Electron microscopy. Muscle specimens were fixed with 2% glutaraldehyde in 0.1 M cacodylate buffer. After shaking with a mixture of 4% osmium tetroxide, 1.5% lanthanum nitrate, and 0.2 M s-collidine for 2–3 hours, samples were embedded in epoxy resin. Semithin sections (1 μm thick) were stained with toluidine blue. Ultrathin sections 50 nm thick were stained with uranyl acetate and lead citrate, then examined under H-600 transmission electron microscope (Hitachi) at 75 kV.

RT-PCR. Total RNA was extracted from biopsied skeletal muscles using TRIzol (Invitrogen), and RT-PCR was performed using SuperScript III (Invitrogen) with random hexamer according to the manufacturer's instructions. Primers for each gene were located on different exons or directly spanning exon-exon boundaries of the genomic sequence in order to minimize amplification from any contaminating genomic DNA. After performing preliminary gradient PCR assays, the optimal annealing temperature for all the primer pairs was determined in order to generate the lowest Ct value as well as a sharp melting peak, with no amplification of nonspecific products or primer-dimer artifacts. Quantitative RT-PCR was performed to compare the mRNA expression of caveoin-1, caveolin-2, caveolin-3, and myostatin using Rotor-Gene 6000 according to the manufacturer's instructions (Corbett Life Science). The reactions were performed in reference to the GAPDH. We used 4 points consisting of 10-fold serial dilution using each primer set to build the standard curve. The PCR reaction (50 cycles) was followed by a melting curve analysis, ranging from 72°C to 95°C, with temperature increasing steps of 0.5°C every 10 seconds. Baseline and threshold values were automatically determined and analyzed. R^2 values exceeded 0.97. The 2-standard curve method was used to determine the relative expression ratio of the target gene in the patient samples versus the control sample, with reference to GAPDH expression.

Cell culture and transfection. COS-7 and C2C12 cells were maintained at 37°C in a humidified atmosphere of 5% CO_2 in DMEM (Sigma-Aldrich) supplemented with 10% fetal bovine serum. Full-length PTRF and caveolin-1 and -3 were amplified using total RNA from control human muscle and cloned into the pGEM-T-easy vector (Promega). The PTRF mutants c.525delG and c.696_697insC were generated using appropriate primers. All primer sequences are shown in Supplemental Table 3.

Immunocytochemistry. COS-7 and C2C12 myoblasts were cotransfected with FLAG-tagged WT or mutant (c.525delG or c.696_697insC) PTRF cDNA and T7-tagged human caveolin-3 using FuGENE6 (Roche). Transfectants were fixed for 30 minutes in 2% paraformaldehyde or 100% methanol, then permeabilized in 0.1% Triton X-100 for 10 minutes. Polyclonal antibodies to FLAG (Sigma-Aldrich) with caveolin-3 (BD Biosciences) or FLAG with β-tubulin (Calbiochem) were applied for double staining.

Immunoprecipitation. COS-7 cells were cotransfected with FLAG-tagged WT or mutant (c.525delG or c.696_697insC) PTRF cDNA and T7-tagged human caveolin-1 or caveolin-3 using FuGENE6 (Roche). The sequences of all constructs were verified with DNA sequencing using ABI PRISM 310 (Applied Biosystems). After 48 hours, the lysates from transfectants were

solubilized with 50 mM Tris-HCl (pH 7.5), 150 mM NaCl, 50 mM EDTA, 1% Triton X-100, and Complete-mini EDTA-free proteinase inhibitors (Roche) (9). The solubilized lysate precleared with Protein G Sepharose (GE Healthcare) was incubated with anti-FLAG (M2; Sigma-Aldrich) and anti-T7 (Novagen) antibodies. Immunoprecipitated proteins were dissociated from beads by boiling in sample buffer and were resolved by SDS-PAGE. Immunoblotting was performed using standard techniques.

Acknowledgments

We thank Sherine Shalaby (Heliopolis Neurocenter, Cairo, Egypt) and May Malicdan (National Center of Neurology and Psychiatry) for reviewing the manuscript. This study was supported by "Research on Psychiatric and Neurological Diseases and Mental Health" of "Health Labour Sciences Research Grant" and by "Research Grant (20B-12, 20B-13) for Nervous and Mental Disorders" from the Ministry of Health, Labor, and Welfare of Japan; by grants from the Human Frontier Science Program; by a Grant-in-Aid for Scientific Research from Japan Society for the Promotion of Science; by Research on Publicly Essential Drugs and Medical Devices from the Japanese Health Sciences Foundation; and by the Program for Promotion of Fundamental Studies in Health Sciences of the National Institute of Biomedical Innovation (NIBIO).

Received for publication January 20, 2009, and accepted in revised form June 3, 2009.

Address correspondence to: Yukiko K. Hayashi, Department of Neuromuscular Research, National Institute of Neuroscience, National Center of Neurology and Psychiatry, 4-1-1 Ogawa-higashi, Kodaira, 187-8502 Tokyo, Japan. Phone: 81-42-341-2711, Fax: 81-42-346-1742; E-mail: hayasi_y@ncnp.go.jp.

1. Scherer, P.E., et al. 1997. Cell-type and tissue-specific expression of caveolin-2. Caveolins 1 and 2 co-localize and form a stable hetero-oligomeric complex in vivo. *J. Biol. Chem.* **272**:29337–29346.
2. Tang, Z., et al. 1996. Molecular cloning of caveolin-3, a novel member of the caveolin gene family expressed predominantly in muscle. *J. Biol. Chem.* **271**:2255–2261.
3. Galbiati, F., Razani, B., and Lisanti, M.P. 2001. Emerging themes in lipid rafts and caveolae. *Cell.* **106**:403–411.
4. Thomas, C.M., and Smart, E.J. 2008. Caveolae structure and function. *J. Cell. Mol. Med.* **12**:796–809.
5. Hill, M.M., et al. 2008. PTRF-Cavin, a conserved cytoplasmic protein required for caveola formation and function. *Cell.* **132**:113–124.
6. Liu, L., et al. 2008. Deletion of Cavin/PTRF causes global loss of caveolae, dyslipidemia, and glucose intolerance. *Cell Metab.* **8**:310–317.
7. Minetti, C., et al. 1998. Mutations in the caveolin-3 gene cause autosomal dominant limb-girdle muscular dystrophy. *Nat. Genet.* **18**:365–368.
8. Matsuda, C., et al. 2001. The sarcolemmal proteins dysferlin and caveolin-3 interact in skeletal muscle. *Hum. Mol. Genet.* **10**:1761–1766.
9. Liu, L., and Pilch, P.F. 2008. A critical role of cavin (polymerase I and transcript release factor) in caveolae formation and organization. *J. Biol. Chem.* **283**:4314–4322.
10. Minetti, C., et al. 2002. Impairment of caveolae formation and T-system disorganization in human muscular dystrophy with caveolin-3 deficiency. *Am. J. Pathol.* **160**:265–270.
11. Ohsawa, Y., et al. 2006. Muscular atrophy of caveolin-3-deficient mice is rescued by myostatin inhibition. *J. Clin. Invest.* **116**:2924–2934.
12. Frost, R.A., and Lang, C.H. 2007. Protein kinase B/Akt: a nexus of growth factor and cytokine signaling in determining muscle mass. *J. Appl. Physiol.* **103**:378–387.
13. Venema, V.J., Ju, H., Zou, R., and Venema, R.C. 1997. Interaction of neuronal nitric-oxide synthase with caveolin-3 in skeletal muscle. Identification of a novel caveolin scaffolding/inhibitory domain. *J. Biol. Chem.* **272**:28187–28190.
14. Sunada, Y., et al. 2001. Transgenic mice expressing mutant caveolin-3 show severe myopathy associated with increased nNOS activity. *Hum. Mol. Genet.* **10**:173–178.
15. Agarwal, A.K., et al. 2002. AGPAT2 is mutated in congenital generalized lipodystrophy linked to chromosome 9q34. *Nat. Genet.* **31**:21–23.
16. Magre, J., et al. 2001. Identification of the gene altered in Berardinelli-Seip congenital lipodystrophy on chromosome 11q13. *Nat. Genet.* **28**:365–370.
17. Kim, C.A., et al. 2008. Association of a homozygous nonsense caveolin-1 mutation with Berardinelli-Seip congenital lipodystrophy. *J. Clin. Endocrinol. Metab.* **93**:1129–1134.
18. Cao, H., Alston, L., Ruschman, J., and Hegele, R.A. 2008. Heterozygous CAV1 frameshift mutations (MIM 601047) in patients with atypical partial lipodystrophy and hypertriglyceridemia. *Lipids Health Dis.* **7**:3.
19. Cao, H., and Hegele, R.A. 2000. Nuclear lamin A/C R482Q mutation in canadian kindreds with Dunnigan-type familial partial lipodystrophy. *Hum. Mol. Genet.* **9**:109–112.
20. Agarwal, A.K., et al. 2003. Phenotypic and genetic heterogeneity in congenital generalized lipodystrophy. *J. Clin. Endocrinol. Metab.* **88**:4840–4847.
21. George, S., et al. 2004. A family with severe insulin resistance and diabetes due to a mutation in AKT2. *Science.* **304**:1325–1328.
22. Barroso, I., et al. 1999. Dominant negative mutations in human PPARgamma associated with severe insulin resistance, diabetes mellitus and hypertension. *Nature.* **402**:880–883.
23. Hegele, R.A., et al. 2006. Sequencing of the reannotated LMNB2 gene reveals novel mutations in patients with acquired partial lipodystrophy. *Am. J. Hum. Genet.* **79**:383–389.
24. Aboulaich, N., Ortegren, U., Vener, A.V., and Stralfors, P. 2006. Association and insulin regulated translocation of hormone-sensitive lipase with PTRF. *Biochem. Biophys. Res. Commun.* **350**:657–661.
25. Razani, B., et al. 2002. Caveolin-1-deficient mice are lean, resistant to diet-induced obesity, and show hypertriglyceridemia with adipocyte abnormalities. *J. Biol. Chem.* **277**:8635–8647.
26. Fulizio, L., et al. 2005. Molecular and muscle pathology in a series of caveolinopathy patients. *Hum. Mutat.* **25**:82–89.
27. Betz, R.C., et al. 2001. Mutations in CAV3 cause mechanical hyperirritability of skeletal muscle in rippling muscle disease. *Nat. Genet.* **28**:218–219.
28. Sugie, K., et al. 2004. Two novel CAV3 gene mutations in Japanese families. *Neuromuscul. Disord.* **14**:810–814.
29. Hayashi, T., et al. 2004. Identification and functional analysis of a caveolin-3 mutation associated with familial hypertrophic cardiomyopathy. *Biochem. Biophys. Res. Commun.* **313**:178–184.
30. Vatta, M., et al. 2006. Mutant caveolin-3 induces persistent late sodium current and is associated with long-QT syndrome. *Circulation.* **114**:2104–2112.
31. Park, D.S., et al. 2002. Caveolin-1/3 double-knockout mice are viable, but lack both muscle and non-muscle caveolae, and develop a severe cardiomyopathic phenotype. *Am. J. Pathol.* **160**:2207–2217.
32. Woodman, S.E., et al. 2002. Caveolin-3 knock-out mice develop a progressive cardiomyopathy and show hyperactivation of the p42/44 MAPK cascade. *J. Biol. Chem.* **277**:38988–38997.
33. Zhao, Y.Y., et al. 2002. Defects in caveolin-1 cause dilated cardiomyopathy and pulmonary hypertension in knockout mice. *Proc. Natl. Acad. Sci. U. S. A.* **99**:11375–11380.
34. Xu, Y., Buikema, H., van Gilst, W.H., and Henning, R.H. 2008. Caveolae and endothelial dysfunction: filling the caves in cardiovascular disease. *Eur. J. Pharmacol.* **585**:256–260.
35. El-Yazbi, A.F., Cho, W.J., Boddy, G., and Daniel, E.E. 2005. Caveolin-1 gene knockout impairs nitrergic function in mouse small intestine. *Br. J. Pharmacol.* **145**:1017–1026.
36. Lobie, P.E., Sadir, R., Graichen, R., Mertani, H.C., and Morel, G. 1999. Caveolar internalization of growth hormone. *Exp. Cell Res.* **246**:47–55.
37. Rajab, A., Heathcote, K., Joshi, S., Jeffery, S., and Patton, M. 2002. Heterogeneity for congenital generalized lipodystrophy in seventeen patients from Oman. *Am. J. Med. Genet.* **110**:219–225.
38. Ghanem, Q. 1993. Percussion myoedema in a Pakistani boy with Berardinelli Seip lipodystrophy syndrome. *Clin. Genet.* **44**:277–278.
39. Simha, V., Agarwal, A.K., Aronin, P.A., Iannaccone, S.T., and Garg, A. 2008. Novel subtype of congenital generalized lipodystrophy associated with muscular weakness and cervical spine instability. *Am J. Med. Genet. A.* **146A**:2318–2326.
40. Kameya, S., et al. 1999. alpha1-syntrophin gene disruption results in the absence of neuronal-type nitric-oxide synthase at the sarcolemma but does not induce muscle degeneration. *J. Biol. Chem.* **274**:2193–2200.

サルコメア配列異常を主病変とする筋ジストロフィーの

病因・病態の解明と治療法の開発

BJ www.biochemj.org

BJ Metabolism

Biochem. J. (2010) **427**, 171–178 (Printed in Great Britain) doi:10.1042/BJ20091346

online data

171

The cathepsin L gene is a direct target of FOXO1 in skeletal muscle

Yoshihiro YAMAZAKI*†‡, Yasutomi KAMEI*[1], Satoshi SUGITA*, Fumiko AKAIKE*, Sayaka KANAI*, Shinji MIURA§, Yukio HIRATA‡, Bruce R. TROEN‖, Tadahiro KITAMURA¶, Ichizo NISHINO**, Takayoshi SUGANAMI*, Osamu EZAKI§ and Yoshihiro OGAWA*†

*Department of Molecular Medicine and Metabolism, Tokyo Medical and Dental University, 1-5-45 Yushima, Bunkyo-ku, Tokyo 113-8510, Japan, †Global Center of Excellence Program, International Research Center for Molecular Science in Tooth and Bone Diseases, Medical Research Institute, Tokyo Medical and Dental University, 1-5-45 Yushima, Bunkyo-ku, Tokyo 113-8510, Japan, ‡Department of Clinical and Molecular Endocrinology, Tokyo Medical and Dental University, 1-5-45 Yushima, Bunkyo-ku, Tokyo 113-8510, Japan, §Nutritional Science Program, National Institute of Health and Nutrition, Tokyo 162-8636, Japan, ‖Geriatrics Research, Education and Clinical Center and Research Service, Miami Veterans Affairs Healthcare System, and Geriatrics Institute, Department of Medicine, Miller School of Medicine, University of Miami, Miami FL 33125, U.S.A., ¶Metabolic Signal Research Center, Institute for Molecular and Cellular Regulation, Gunma University, Maebashi, Gunma 371-8512, Japan, and **Department of Neuromuscular Research, National Institute of Neuroscience, National Center of Neurology and Psychiatry, Tokyo 187-8502, Japan

FOXO1 (forkhead box O1), a forkhead-type transcription factor whose gene expression is up-regulated in the skeletal muscle during starvation, appears to be a key molecule of energy metabolism and skeletal muscle atrophy. Cathepsin L, a lysosomal proteinase whose expression is also up-regulated in the skeletal muscle during starvation, is induced in transgenic mice overexpressing FOXO1 relative to wild-type littermates. In the present study, we conducted *in vivo* and *in vitro* experiments focusing on FOXO1 regulation of *Ctsl* (cathepsin L gene; *CTSL1* in humans) expression in the skeletal muscle. During fasting and refeeding of C57BL/6 mice, *Ctsl* was regulated in parallel with FOXO1 in the skeletal muscle. Fasting-induced *Ctsl* expression was attenuated in transgenic mice overexpressing a dominant-negative form of FOXO1 or in skeletal-muscle-specific *Foxo1*-knockout mice relative to respective wild-type controls. Using C2C12 mouse myoblasts overexpressing a constitutively active form of FOXO1, we showed that FOXO1 induces *Ctsl* expression. Moreover, we found FOXO1-binding sites in both the mouse *Ctsl* and human *CTSL1* promoters. The luciferase reporter analysis revealed that the mouse *Ctsl* and human *CTSL1* promoters are activated by FOXO1, which is abolished by mutations in the consensus FOXO1-binding sites. Gel mobility-shift and chromatin immunoprecipiation assays showed that FOXO1 is recruited and binds to the *Ctsl* promoter. The present study provides *in vivo* and *in vitro* evidence that *Ctsl* is a direct target of FOXO1 in the skeletal muscle, thereby suggesting a role for the FOXO1/cathepsin L pathway in fasting-induced skeletal muscle metabolic change and atrophy.

Key words: atrophy, cathepsin L, forkhead box O1 (FOXO1), forkhead transcription factor, muscle metabolism, starvation.

INTRODUCTION

The skeletal muscle is the largest organ in the human body, with important roles in exercise, glucose uptake and energy expenditure. Skeletal muscle metabolism is changed by the supply of nutrients and circulating hormones [1,2]. Starvation and disease states (such as diabetes and cancer cachexia) lead to a rapid reduction in skeletal muscle mass (atrophy) [2]. What is the physiological role of muscle atrophy? As the brain mainly uses glucose as an energy source, during starvation it needs to be supplied with glucose. Thus, for short periods of fasting, skeletal muscle increases utilization of lipids instead of glucose. On the other hand, for longer periods of fasting or starvation resulting in muscle atrophy, skeletal muscle protein is degraded and mobilized as a source of amino acids for gluconeogenesis that occurs mainly in the liver [3].

The FOXO (forkhead box O) members FOXO1, FOXO3a and FOXO4 belong to a subfamily of the forkhead transcription factors [4,5]. The FOXO family regulates a variety of biological processes such as metabolism, cell proliferation, apoptosis, stress response and longevity [6–9]. FOXO1 activates gluconeogenic enzyme genes in the liver, such as those for PEPCK (phosphoenolpyruvate carboxykinase) and G6Pase (glucose-6-phosphatase). A dominant-negative form of FOXO1 (DN-FOXO1), which contains the DNA-binding domain, but lacks the transcriptional activation domain, suppressed the fasting-induced increase of *Pepck* and *G6Pase* expression in liver cells [10]. We showed previously that energy-deprived conditions in mice, such as fasting and diabetes, up-regulated expression of *Foxo1* in skeletal muscle of mice [11]. Several FOXO1 target genes have been identified in skeletal muscle. For instance, FOXO1 up-regulates *PDK4* (pyruvate dehydrogenase kinase 4), a kinase that suppresses glycolysis [12], and *LPL* (lipoprotein lipase), an enzyme that increases lipid incorporation [11], and down-regulates *SREBP1c* (sterol-regulatory-element-binding protein 1c), a master regulator of lipogenesis [13]. The FOXO1 target genes may be involved in the utilization of lipids instead of glucose in the skeletal muscle. On the other hand, forced expression of FOXO1 or FOXO3a up-regulates the expression of a variety of atrophy-related genes including the *MuRF1* and *atrogin/MAFbx* ubiquitin ligases [14,15], as well as *Bnip3* and *LC3*, important molecules for autophagy [16,17], thus inducing skeletal muscle atrophy *in vitro* and *in vivo*. We have created transgenic mice that overexpress FOXO1 in skeletal muscle (FOXO1 mice) and found

Abbreviations used: ChIP, chromatin immunoprecipitation; DBE, DAF16 (decay-accelerating factor 16)-binding element; DMEM, Dulbecco's modified Eagle's medium; DN-FOXO1, dominant-negative forkhead box O1; ER, oestrogen receptor; FBS, fetal bovine serum; FOXO, forkhead box O; GADD45α, growth-arrest and DNA-damage-inducible protein 45α; G6Pase, glucose-6-phosphatase; HEK, human embryonic kidney; PEPCK, phosphoenolpyruvate carboxykinase; PLSD, protected least-significant difference; TAM, tamoxifen.

[1] To whom correspondence should be addressed (email kamei.mmm@mri.tmd.ac.jp).

that they exhibit skeletal muscle atrophy [18]. Moreover, FOXO1 has been shown to induce *Gadd45a* (growth-arrest and DNA-damage-inducible protein 45α) [19], a suppressor of the cell cycle, thereby facilitating skeletal muscle atrophy. Thus identification and functional analysis of FOXO1 target genes will help facilitate a better understanding of skeletal muscle metabolism.

Cathepsin L is a lysosomal proteinase, whose expression is up-regulated during various forms of skeletal muscle atrophy including starvation [20–22]. In the skeletal muscle of the FOXO1 mice, *Ctsl* expression was markedly increased [18]. Earlier findings showed that lysosomal proteolysis is activated upon skeletal muscle atrophy [23,24]. Although circumstantial evidence suggests that cathepsin L is involved in skeletal muscle atrophy, to our knowledge, there are no reports on the regulation of *Ctsl* by FOXO1. In the present study, we provide *in vivo* and *in vitro* evidence that *Ctsl* is a direct target of FOXO1 in skeletal muscle.

EXPERIMENTAL

Genetically modified animals

The human skeletal muscle α-actin promoter [25] was kindly provided by Dr E.C. Hardeman and Dr K. Guven (Children's Medical Research Institute, Westmead, NSW, Australia). DN-FOXO1, a mutant version of FOXO1 containing amino acid residues 1–256, has been described previously [26]. Transgenic plasmid containing the cDNA for DN-FOXO1 (see Figure 2A) was excised and purified for injection (at $2\,ng \cdot \mu l^{-1}$) [18]. Fertilized eggs were recovered from C57BL/6 females crossed with C57BL/6 males and microinjected at Japan SLC Inc. (Hamamatsu, Japan). To obtain skeletal-muscle-specific *Foxo1*-knockout mice, we inactivated *Foxo1* expression in the skeletal muscle by crossing mice homozygous for a floxed *Foxo1* allele with myogenin-cre transgenics. Myogenin-cre and *Foxo1*^{flox} mice were as described previously [27]. The mice were maintained at a constant temperature of 24 °C with fixed artificial light (12 h light/12 h dark). All animal experiments were conducted in accordance with the guidelines of Tokyo Medical and Dental University Committee on Animal Research (No. 0090041) and National Institute of Health and Nutrition (No. 0706).

C2C12 cells and cell cultures

C2C12 mouse myoblasts (RIKEN Cell Bank, Tsukuba, Japan) were cultured in DMEM (Dulbecco's modified Eagle's medium) containing 10 % (v/v) FBS (fetal bovine serum) until the cells reached confluence. The medium was then replaced with DMEM containing 2 % (v/v) horse serum (differentiation medium) and incubated for 4 days to induce the formation of myotubes before each experiment. C2C12 myoblasts stably expressing FOXO1–ER (oestrogen receptor) fusion proteins were obtained as described previously [28]. In brief, C2C12 cells were stably transfected with the empty pBABE retrovirus or pBABE vectors expressing fusion proteins containing a constitutively active form of human FOXO1 [FOXO1(3A)] [26] [where three Akt phosphorylation sites (Thr^{24}, Ser^{256} and Ser^{319}) are replaced by alanine residues] in-frame with a modified TAM (tamoxifen)-specific version of the murine ER-ligand-binding domain. FOXO1–ER plasmid was provided by Dr Terry G. Unterman (Department of Medicine, University of Illinois at Chicago, U.S.A.) Cells were selected with puromycin and colonies were pooled for studies, as reported previously [13]. The fusion proteins are restricted to the cytoplasmic space until activation by treatment with TAM [28].

Quantitative real-time PCR

Quantitative real-time PCR was performed as described previously [13]. Total RNA was prepared using Sepazol. cDNA was synthesized from 5 μg of total RNA using ReverTra Ace® (TOYOBO) with random primers. Gene expression levels were measured with an ABI PRISM 7700 Sequence Detection System using SYBR Green PCR Core Reagents (Applied Biosystems). Levels of mRNA were normalized to those of *36B4* mRNA. The primers used were as follows. Cathepsin L: forward, 5′-TCTCACGCTCAAGGCAATCA-3′, reverse, 5′-AAGCAAAATCCATCAGGCCTC-3′; GADD45α: forward, 5′-CGTAGACCCCGATAACGTGGTA-3′, reverse, 5′-CGGATGAGGGTGAAATGGAT-3′; FOXO1: forward, 5′-ATTCGGAATGACCTCATGGA-3′, reverse, 5′-GTGTGGGAAGCTTTGGTTGG-3′; DN-FOXO1 (transgene specific): forward, 5′-GACTACAAGGACGACGATGA-3′, reverse, 5′-AGCGGCTCGAAGTCCGGGTC-3′, FOXO3a: forward, 5′-TCTGCGGGCTGGAAGAACT-3′, reverse, 5′-CTCTTGCCCGTGCCTTCAT-3′; FOXO4: forward, 5′-ATGGATGGTCCGCACGGTG-3′, reverse, 5′-CTTGCCAGTGGCCTCGTTG-3′; and 36B4: forward, 5′-GGCCCTGCACTCTCGCTTTC-3′, reverse 5′-TGCCAGGACGCGCTTGT-3′.

Cloning of the mouse *Ctsl* and human *CTSL1* promoters

The mouse *Ctsl* promoter has been described previously [29]. The 4-kb mouse *Ctsl* promoter region was excised with BamHI from pMEPCAT3 and cloned into a pGL3-basic luciferase vector (Promega Corporation). The 4-kb mouse promoter was sequenced. The human *CTSL1* promoter [30,31] was obtained by PCR from genomic DNA of HEK (human embryonic kidney)-293 cells. The PCR primers used were 5′-GTGGTGCGCGCCTGTAGTCC-3′ and 5′-GGCGCACTCCACGGATGCCG-3′. Mutations in the promoter sequences were introduced using a QuikChange® site-directed mutagenesis kit (Stratagene). Primers used were human DBE1: 5′-CTGGGACAGTCAGTGGGCAAGCCACGAACC-3′; human DBE2: 5′-GGGACAGTCAGTGGGCAAGCCACGAACC-3′; and mouse DBE: 5′-GTGATAGACTGAGTGGGCAAACATACAAAG-3′. DBE is DAF16 (decay-accelerating factor 16)-binding element, to which FOXO1 binds [32].

Transfection and luciferase assay

HEK-293 cells were plated at a density of 10^5 cells/12-well plate in DMEM containing 10 % (v/v) FBS. Luciferase gene constructs containing a *Ctsl* promoter fragment with or without mutations of putative FOXO1-binding sites were prepared. The luciferase reporter plasmid (0.8 μg), the expression plasmid [pCAG-FOXO1(3A) or empty pCAG, 0.8 μg], and a phRL-TK vector (25 ng; Promega) as an internal control for transfection efficiency, were transfected into HEK-293 cells using Lipofectamine™ 2000 (Invitrogen). After an overnight transfection period, cells were lysed and assayed for luciferase activity using the dual-luciferase assay kit (Promega). The activity was calculated as the ratio of firefly luciferase activity to *Renilla* luciferase activity (internal control) and expressed as the average of triplicate experiments.

Gel mobility-shift assay

The gel mobility-shift assay was performed as described previously [33]. *In-vitro*-translated human FOXO1 was generated from pCMX-FOXO1, using the TNT® T7

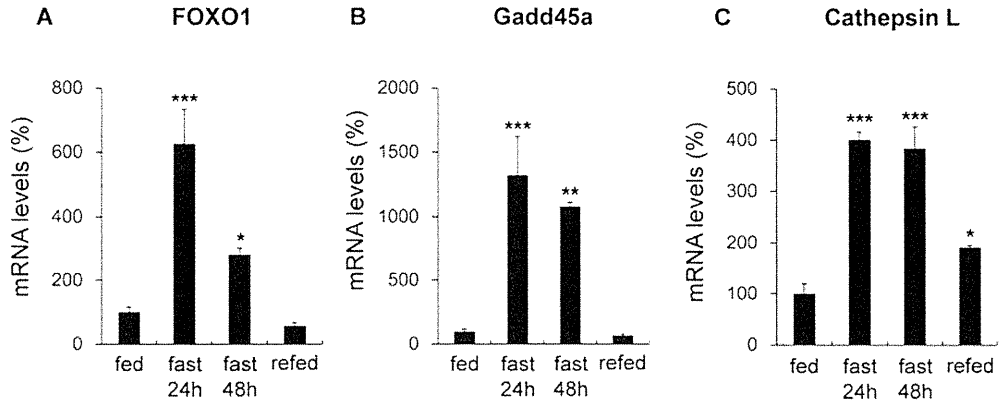

Figure 1 ***Foxo1*, *Gadd45a* and *Ctsl* expression in skeletal muscle of fasted and refed mice**

Mice (C57BL6, male, 8 weeks of age) were divided into four experimental groups of four mice each. They were either allowed to eat freely (fed), or subjected to a 24 or a 48 h fast. Others were subjected to a 48 h fast followed by 8 h of feeding (refed). Mice were killed, and relative mRNA levels of *Foxo1* (endogenous), *Gadd45a* and *Ctsl* in skeletal muscle (gastrocnemius) were analysed by quantitative real-time PCR. Levels of mRNA were normalized to those of *36B4* mRNA. Values of fed samples were set at 100. $^{*}P < 0.05$, $^{**}P < 0.01$; and $^{***}P < 0.001$ compared with the fed group.

Quick Coupled Transcription/Translation System (Promega) according to the manufacturer's instruction. Double-stranded oligonucleotide probes used in gel mobility-shift assays were prepared by annealing both strands of each putative FOXO1-binding site in the human *CTSL1* promoter (DBE1: 5′-ATCTCCAAAATAGTAAACAAATTCCTGCAG-3′, −145 to −152, numbering the first nucleotide of exon 1 as +1; DBE2: 5′-GGGACAGTCAGTAAACAAGCCACGAACC-3′, −1400 to −1407, numbering the first nucleotide of exon 1 as +1; DBE1 mutant: 5′-ATCTCCAAAATAGTGGGCAA-ATTCCTGCAG-3′; and DBE2 mutant: 5′-GGGACAGTC-AGTGGGCAAGCCACGAACC-3′; underlining indicates sites of mutation) and labelling with [γ-^{32}P]ATP (PerkinElmer Life Sciences) using T4 polynucleotide kinase (Roche Applied Science). The labelled probes (50000 d.p.m.) were incubated with extracts containing *in-vitro*-translated FOXO1 in a mixture (total volume of 25 μl) containing 10 mM Tris/HCl (pH 7.5), 50 mM NaCl, 1 mM DTT (dithiothreitol), 1 mM EDTA and 4.4% glycerol with 1 mg of poly(dI-dC)·(dI-dC) for 30 min on ice and then separated by electrophoresis on a 6% polyacrylamide gel in 45 mM Tris/HCl (pH 8.0), 45 mM borate and 1 mM EDTA. After electrophoresis, gels were dried and analysed with a BAS-2500 (Fuji Film).

ChIP (chromatin immunoprecipitation) assay

ChIP was carried out using a ChIP assay kit (Upstate Biotechnology) according to the manufacturer's guidelines [13,34]. Briefly, C2C12 myoblasts stably expressing FOXO1(3A)–ER were incubated for 24 h with or without 1 μM TAM. Proteins were cross-linked to DNA with the addition of formaldehyde (1% final concentration). Cells were washed and lysed in SDS lysis buffer, sonicated for 10 s and allowed to recover for 30 s over ice (this was repeated seven times). Lysates were cleared with Protein A–agarose for 30 min, pelleted and incubated overnight with an anti-FOXO1 antibody (sc-11350; Santa Cruz Biotechnology). Before the incubation, input samples were removed from the lysate and stored at 4°C until extraction. Following incubation with the antibody, protein–DNA complexes were eluted (1% SDS and 0.1 M $NaHCO_3$), and the cross-links were reversed. DNA was purified by phenol/chloroform extraction. PCR primers were designed to locate DBE of the *Ctsl* promoter: forward, 5′-AAAAGACAAGAGGATGCCTT-3′, and reverse, 5′-CTGGTGTTCTCAGGTTAGTC-3′. The amplified region was −3670 to −3339, numbering the first nucleotide of exon 1 as +1. PCR primers were also designed to locate non-DBE of the *Ctsl* promoter: forward, 5′-CCACGAAAAGAATTTCTACCA-3′ and reverse, 5′-AGTTGTAGATTAAAATGTGCAG-3′. The amplified region was −439 to −289, numbering the first nucleotide of exon 1 as +1.

Statistical analysis

All results are expressed as means ± S.E.M. Statistical comparisons of data from experimental groups were made with a one-way ANOVA, and groups were compared using Fisher's PLSD (protected least-significant difference) test (Statview 5.0; Abacus Concepts, Berkeley, CA, U.S.A.). When differences were significant, groups were compared using Fisher's PLSD test. Statistical significance was defined as $P < 0.05$.

RESULTS

Co-ordinate regulation of *Foxo1* and *Ctsl* expression in the mouse skeletal muscle during fasting and refeeding

To analyse the *in vivo* relationship between *Foxo1* and *Ctsl* expression, we first examined their gene expression in the skeletal muscle of mice subjected to fasting and refeeding. Expression of mRNAs for *Foxo1* and *Gadd45a*, a *bona fide* FOXO1-target gene [19], was increased in skeletal muscle after 24 and 48 h of fasting (Figures 1A and 1B). *Ctsl* mRNA expression was also markedly increased in the skeletal muscle during fasting (Figure 1C). The effect of fasting was reversed by refeeding. *Foxo1* and *Ctsl* mRNA levels were increased in various regions of skeletal muscles, such as gastrocnemius (Figure 1), soleus, extensor digitorum longus and tibialis anterior (see Supplementary Figure S1 at http://www.BiochemJ.org/bj/427/bj4270171add.htm). In other tissues, such as the brain, kidney and adipose tissue, fasting did not markedly alter *Foxo1* and *Ctsl* mRNA expression (Y. Kamei, unpublished work). These observations indicate that the expression of *Foxo1* and *Ctsl* is co-ordinately regulated in the skeletal muscle during fasting and refeeding.